CZECH TECHNICAL UNIVERSITY IN PRAGUE

Faculty of Electrical Engineering

Department of Measurements

Excitation Unit for Orthogonal Fluxgate with DC Bias Flipping

Bachelor Thesis

Study Programme: Cybernetics and Robotics

Branch of study: Systems and Control

Thesis supervisor: Ing. Mattia Butta, PhD

Iurie Coroli

Prague, 2016

Czech Technical University in Prague
Faculty of Electrical Engineering

Department of Control Engineering

BACHELOR PROJECT ASSIGNMENT

Student: **Iurie Coroli**

Study programme: Cybernetics and Robotics

Specialisation: Systems and Control

Title of Bachelor Project: **Excitation unit for orthogonal fluxgate with dc bias flipping**

Guidelines:

1. Orthogonal fluxgate in flundamental mode are very precise sensors of magnetic field. However, they often present a large bias due to non-perfectly circumferential magnetic anisotropy.
2. The offset can be suppressed by periodical flipping of dc bias, however this can introduce some spurios noise in the output the sensor.
3. The goal of this project is to develop a precise exctation unit for this sensor based on DDS technology for generation of high purity sinewave excitaion and simultaneously implementation of dc bias flipping controllable by external signal.
4. Then the student will create a system synchronizing the developped excitation unit with PXI data acuisition module and he will develop an algorithm for compensation of spurios noise after dc bias flipping.

Bibliography/Sources:

[1] Butta M., Sasada I.: Method for offset suppression in orthogonal fluxgate with annealed wire core. Sensor Letters. 2014, no. 12, p. 1295-1298.
[2] Sasada I, Usui T.: Orthogonal Fluxgate Magnetometer Utilizing Bias Switching for Stable Operation, Sensors, 2003. Proceedings of IEEE, Vol. 1, 468 - 471 , 22-24 Oct. 2003
[3] Datasheet of AD9850: http://www.analog.com/media/en/technical-documentation/data-sheets/AD9850.pdf

Bachelor Project Supervisor: Ing. Mattia Butta, Ph.D.

Valid until the summer semester 2016/2017

L.S.

prof. Ing. Michael Šebek, DrSc.
Head of Department

prof. Ing. Pavel Ripka, CSc.
Dean

Prague, January 11, 2016

Acknowledgement

I would first like to thank my thesis advisor Ing. Mattia Butta, PhD, for his assistance and dedicated involvement in every step throughout the process. Without his great mentorship this paper would have never been accomplished. I would also like to thank my family and friends for their moral support and help.

I hereby declare that I have completed this thesis with the topic "Excitation unit for orthogonal fluxgate with dc bias flipping" independently and that I have included a full list of used references. I have no objection to the usage of this work in compliance with the act §60 Zákon č.121/2000 Sb. (copyright law).

In.....Date.....

Signature of the author

Table of Contents

Abstract

The goal of this bachelor thesis is to develop a system for suppression of the offset and its temperature drift in an orthogonal fluxgate in fundamental mode. The offset is generally high, unstable and has a large thermal drift, which results in a large low-frequency noise. We propose a system that periodically flips the polarity of both DC and AC excitation currents to overcome this issue. The polarity flipping however introduces transients and additional noise at larger frequency; we overcome this issue by digital signal processing, excluding the first periods after polarity flipping from integration. We managed to achieve thermal offset variation of about 0.015 nT/°C with tolerable increase of the noise floor at high frequency. The achieved offset stability and low noise floor are comparable to top class available fluxgates. Such combination of characteristics has never been achieved on a cheap fluxgate sensor so far. Moreover, we have low power consumption because we use low excitation current below 100 mA and there is no need for expensive electronics.

Keywords

Orthogonal fluxgate, polarity flipping, low noise, offset drift, magnetic sensors, temperature stability

Abstrakt

Cílem této práce je navrhnout systém pro potlačení offsetu a jeho teplotního posunu ortogonálního fluxgate sensoru ve fundamentálním modu. Obvykle offset je velký, nestabilní a má nezanedbatelný teplotní posun, kvůli tomu vzniká nízkofrekvenční šum. V této práce bude navrhnut systém, který periodický mění polaritu budicích AC a DC proudů pro řešení úkolu práce. Avšak měnicí polarita vyvolává přechodové jevy a vysokofrekvenční šum. Tento problém bude řešen pomoci digitálního zpracování signálů tím že vynecháme z přijímaných dat první periodu po přepnutí polarity. Dokázali jsme dosáhnout veličiny termálního posunu offsetu kolem 0.015 nT/°C při tolerovaném nárůstu úrovně vysokofrekvenčního šumu. Dosazená stabilita offsetu a nízký úroveň šumu lze porovnávat s fluxgate sensory nejvyšší třidy. Takové charakteristiky nebyli nikdy dosažené u levných fluxgate sensorů. Kromě toho sensor použitý při tvořeni práce má nízkou spotřebu, protože byl použit malý budicí proud do 100 mA.

Klíčová slova

Ortogonální fluxgate, přepnutí polarity, nízký úroveň šumu posun offsetu, magnetický sensor, teplotní stabilita

I. State of the art

1. Introduction to magnetic sensors

Magnetic sensors are used to measure magnetic field and are applied in various areas: archeology, resources exploration, space exploration, probing Earth magnetosphere, military etc.

It is convenient to start description of magnetic field sensors by stating Faraday's law. Let us have a simple magnetic field sensor – conducting coil with some core inside. Then if there is magnetic field present in the core, there will be voltage induced according to the following equation:

$$V_i = -\frac{d\Phi}{dt} = -N\frac{d(\vec{B}\cdot\vec{S})}{dt} = -\frac{d(N\mu_0\mu_r\vec{H}\cdot\vec{S})}{dt}, \text{ where} \quad (1)$$

N – number of turns in the coil,

μ_0 – permeability of free space

μ_r – relative permeability of the sensor core

$\vec{H}$ – magnetic field in the sensor core

$\vec{S}$ – cross-sectional area of the core

If we assume $\vec{S}$ and μ_r are constant in time, then equation (1) becomes

$$V_i = -N\mu_0\mu_r\vec{S}\cdot\frac{d\vec{H}(t)}{dt}. \quad (2)$$

1.1 Regular search coil

From the equation (2) it follows that for the basic induction coils

$$\int_{t_1}^{t_2} V_i\,dt = -\left(N\mu_0\mu_r\vec{H}_{t2}\cdot\vec{S} - N\mu_0\mu_r\vec{H}_{t1}\cdot\vec{S}\right). \quad (3)$$

We can see that in such way we do not measure DC field. Hence search coils are only used for high frequency field variations. They also cannot be used when high precision is required because of their low sensitivity. However search coils are relatively easy to operate as they do not require low temperature or complex electronics, and are compact and cheap. Currently they are used for eye-tracking, auroral substorm measurements etc.

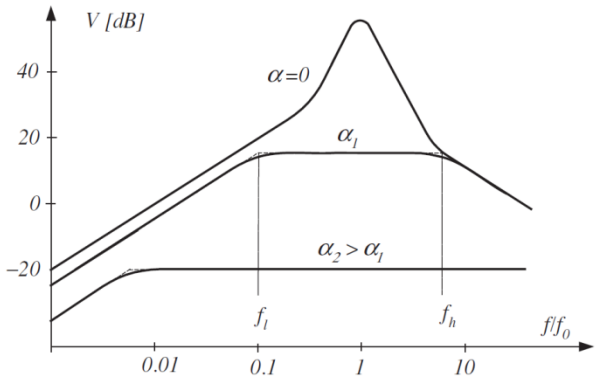

Figure 1: Frequency response of search coil magnetometer [1].

1.2 SQUID

Most of other magnetic field sensors on contrary are good at measuring low-frequency magnetic fields. The best currently existing sensor is SQUID – Superconducting Quantum Interference Device. They are based on superconducting loops containing Josephson junctions. SQUIDs can measure fields order of 5 aT ($5 \cdot 10^{-18}\,T$), but the tradeoff for the excellent sensitivity is operation at very low temperature (typical value 77 K) and complexity of driving electronics. SQUIDS are used in medical equipment (MEG, cardiology, MRI), measurement of magnetic properties of materials, SQUID microscope etc. [2]

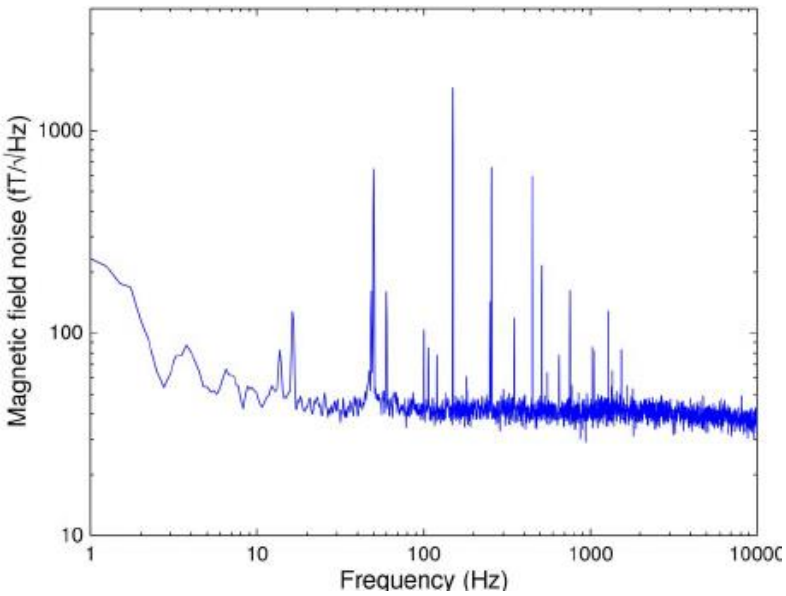

Figure 2.: Magnetic noise of high-Tc SQUID [3].

Fluxgate provides a good resolution order of 10 pT and is relatively easy to operate.

2. Orthogonal fluxgate

Fluxgate is a widely used magnetic field sensor because it provides high resolution measurement of magnetic field at room temperature. There are two types of fluxgates: parallel and orthogonal.

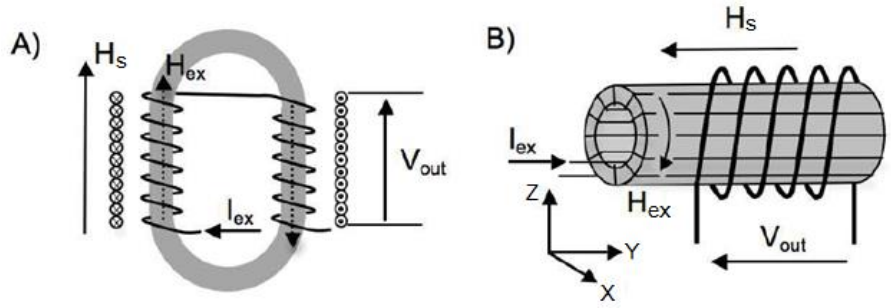

Figure 3: a) Parallel fluxgate sensor b) Orthogonal fluxgate sensor [4].

In a fluxgate we have a core of ferromagnetic material periodically saturated in opposite directions by an excitation field. In a parallel fluxgate an excitation coil is wound around the core in such a way that it produces excitation field H_{EX} parallel to sensed magnetic field H_S. An orthogonal fluxgate – in its simplest form – is composed of cylindrical ferromagnetic core, a toroidal excitation winding and a pick-up coil wound around it; excitation field H_{EX} is a circular field. H_{EX} is located in the XZ-plane, while the sensed field H_S is located in the –Y direction, therefore H_{EX} and H_S are orthogonal.

In order to explain the working principle of orthogonal fluxgate let us consider an isotropic ferromagnetic core exposed to excitation field H_{ex} and sensed field H_s. The latter is constant, or at much lower frequency than H_{EX}, and the former is produced by sine wave signal in the excitation coil (for practical applications other waveforms are used to reduce the power consumption). We assume that H_s is much smaller than H_{ex} and much smaller than the saturation filed H_{sat}. The total magnetic field is then

$$H_{tot} = \sqrt{\left({H_{ex}}^2 + {H_s}^2\right)}. \qquad (4)$$

If H_{tot} is lower than saturation field H_{sat} magnetization vector M is codirectional with H_{tot} and $M_y=H_y$. This can be derived from the fact that field energy

$$E_{tot} = -\mu_0 \vec{M} \cdot \vec{H} \qquad (5)$$

has to be minimized [5]. Because of the negative sign, the minimum energy E_{tot} is reached when $\vec{M} \cdot \vec{H}$ is maximal, i.e. when the two vectors are codirectional. In this mode if the circumferential field H_{ex} rises M rotates with vector H_{tot} and increases its amplitude keeping M_y constant because H_y is constant. When H_{tot} reaches H_{sat} the magnetization vector M starts rotating on a circumference corresponding to $M=M_{sat}$ and M_y is no longer directly proportional to H_y. The operation principle is symmetric in the negative saturation. The voltage induced in the pickup coil is then proportional to time derivative of M_y, the output signal is at the second and higher order even harmonics, because there are two drops of M_y per period of excitation current.

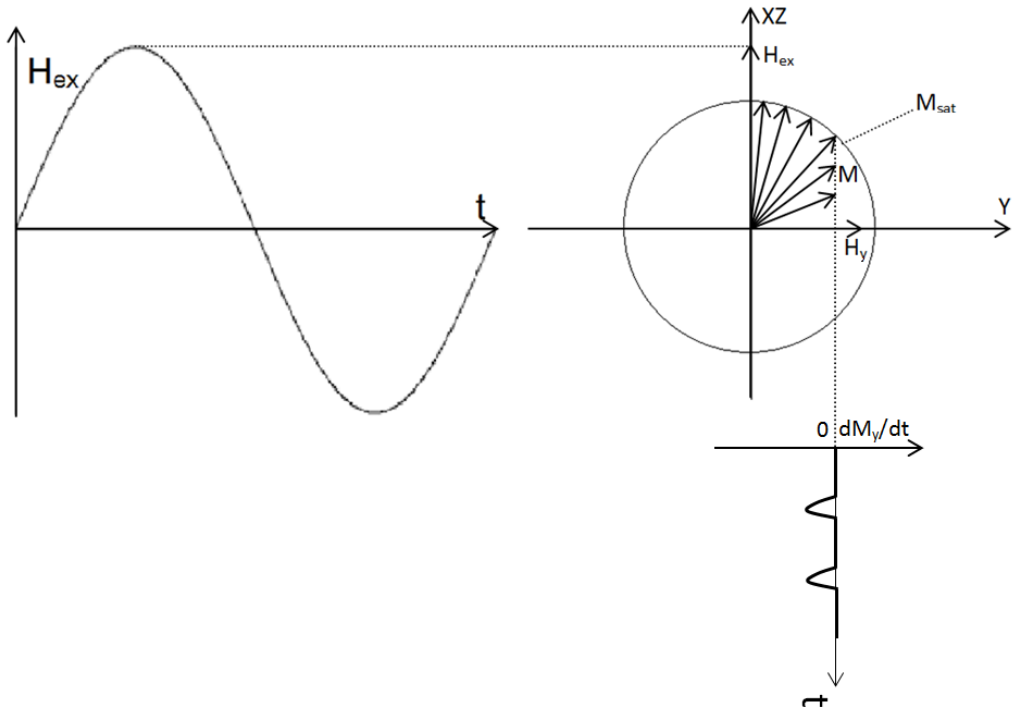

Figure 4: Working principle of orthogonal fluxgate.

If H_y is larger, then the value of M_y is larger and M_{sat} is reached earlier and the integral of the induced voltage will be larger.

The fluxgate mechanism is explained in more details in [6].

2.1 Fundamental mode of orthogonal fluxgate

In 2002 Sasada proposed fundamental mode of orthogonal fluxgate [7]. The structure of the sensor remained the same, only the operating mode changed. The difference is that a large DC bias is added to the AC excitation current. The purpose of the bias is to keep the core always saturated in one direction; therefore the value of the DC bias depends on the magnetic properties of a particular core, that is the value of the DC bias should be chosen so that the resulting minimum value of the excitation field is still in the saturated region of the B-H loop. Most of the noise in fluxgate sensors comes from Barkhausen noise originated from the magnetization switching from one saturated state to the opposite [8]. Keeping the fluxgate always saturated in one direction gradually decreases its noise.

Let us consider an isotropic wire excited by circumferential field $H_{DC}+H_{AC}$, generated by the excitation current. If there is no sensed field present in y-direction then M is simply oriented circumferentially and the magnitude corresponds to maximal magnetization M_S (Figure 5).

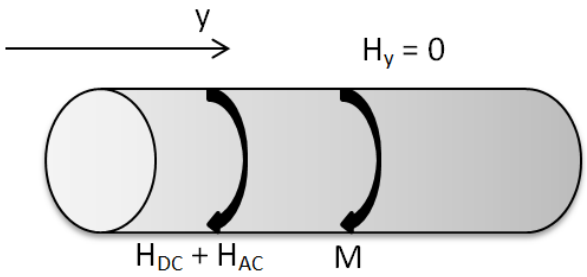

Figure 5: Ferromagnetic core of orthogonal fluxgate in fundamental mode, no external field H_y is present.

However, if external field H_y is present the magnetization amplitude is still M_S but it is deflected from circumferential direction by some angle α. The angle depends on the amplitude of $(H_{DC} + H_{AC})$ and H_y. It is possible to observe how α behaves if we consider the total field energy

$$E_{tot} = -\mu_0 M(H_{DC} + H_{AC})\cos\alpha - \mu_0 M H_y \cos\left(\frac{\pi}{2} - \alpha\right). \quad (6)$$

The magnetization vector tends to take the position associated with minimal field energy. When the H_{AC} reaches its maximal value the total circumferential field is $H_{DC} + |H_{AC}|$ and α is minimal; when H_{AC} is minimal the total circumferential field is $H_{DC} - |H_{AC}|$ and α is maximal. It is possible to derive the value of α analytically:

$$\frac{\partial E_{tot}}{\partial \alpha} = \mu_0 M (H_{DC} + H_{AC}) \sin\alpha - \mu_0 M H_y \sin\left(\frac{\pi}{2} - \alpha\right) = 0. \quad (7)$$

Taking into account that $\sin\left(\frac{\pi}{2} - \alpha\right) = \cos\alpha$ it follows from (7) that

$$\alpha = \operatorname{atan}\left(\frac{H_y}{H_{DC} + H_{AC}}\right). \quad (8)$$

The second derivative of energy with respect to angle between magnetization and excitation magnetic field is

$$\frac{\partial^2 E_{tot}}{\partial \alpha^2} = \mu_0 M H_{ex} \cos\alpha - \mu_0 M H_y \sin\alpha = \mu_0 M H_{ex} \sqrt{1 + \left(\frac{H_y}{H_{ex}}\right)^2} > 0. \quad (9)$$

Hence the minimal energy is achieved at $\alpha = \operatorname{atan}\left(\frac{H_y}{H_{DC}+H_{AC}}\right)$.

The projection of M on the y-axis which is $M \cdot \sin\alpha$ oscillates with the same frequency as H_{AC}. The voltage induced in the pick-up coil is proportional to the time derivative of M_y. M oscillates at the same frequency as H_{AC}, therefore the output signal is now at the fundamental frequency.

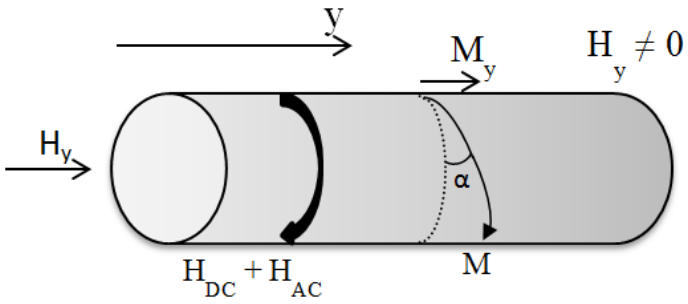

Figure 6: Ferromagnetic core of orthogonal fluxgate in fundamental mode, external field Hy is present.

Let us consider a sensed magnetic field H_y, an excitation AC current of amplitude I_{AC} and DC current I_{DC}. Let the sensor ferromagnetic core have radius R. The magnetic field strength created by current I in a wire at its edge is given by Ampere's law

$$H = \frac{I}{2\pi R}. \qquad (10)$$

The excitation circumferential magnetic field is then given by

$$H_{AC} + H_{DC} = \frac{I_{DC} \pm I_{AC}}{2\pi R}, \qquad (11)$$

where "+" sign corresponds to positive part of the period and "-" sign corresponds to negative part of the period. The angle between the vector of magnetization and XZ-plane is given by (8). The projection of $\vec{M}$ on the Y-axis is given by $M \sin\alpha$ and the peak-to-peak value of the variations of M_y is given by

$$M_{y(pp)} \propto \sin\alpha_1 - \sin\alpha_2 = \sin\left[\operatorname{atan}\left(\frac{2\pi R H_y}{I_{DC} - I_{AC}}\right)\right] - \sin\left[\operatorname{atan}\left(\frac{2\pi R H_y}{I_{DC} + I_{AC}}\right)\right]. \qquad (12)$$

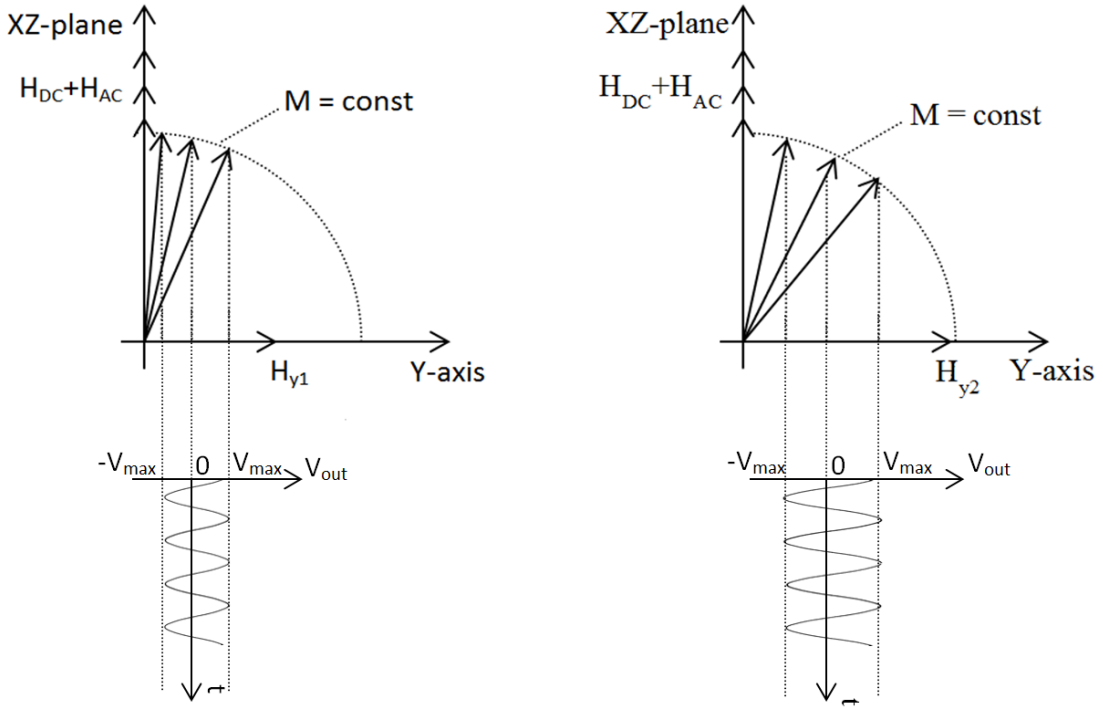

Figure 7: Working principle of fundamental mode orthogonal fluxgate. Here $H_{y2} > H_{y1}$ and as a consequence the output signal has larger amplitude.

The output voltage is proportional to variations of projection of $\vec{M}$ on the axis of cylindrical ferromagnetic core, M_y. Since $M_y = \vec{M} \cdot \sin\alpha$ (α measured from the XZ-plane) the peak-to-peak value of output voltage is proportional to $(\sin\alpha_{max} - \sin\alpha_{min})$, where α_{max} is the maximal angle of deflection of $\vec{M}$ (reached at minimal excitation field) and

α_{min} is minimal angle of inclination (reached at maximal excitation field). The resulting sensitivity curve can be found in Figure 8. The vertical axis represents the normalized output voltage amplitude. The horizontal axis represents the magnitude of magnetic field strength in y-direction of the sensor. The sensitivity curve was calculated using H_{EX} varying from 80 A/m to 185 A/m and core radius R = 60 μm as typical value for the magnetic wires used for such sensors.

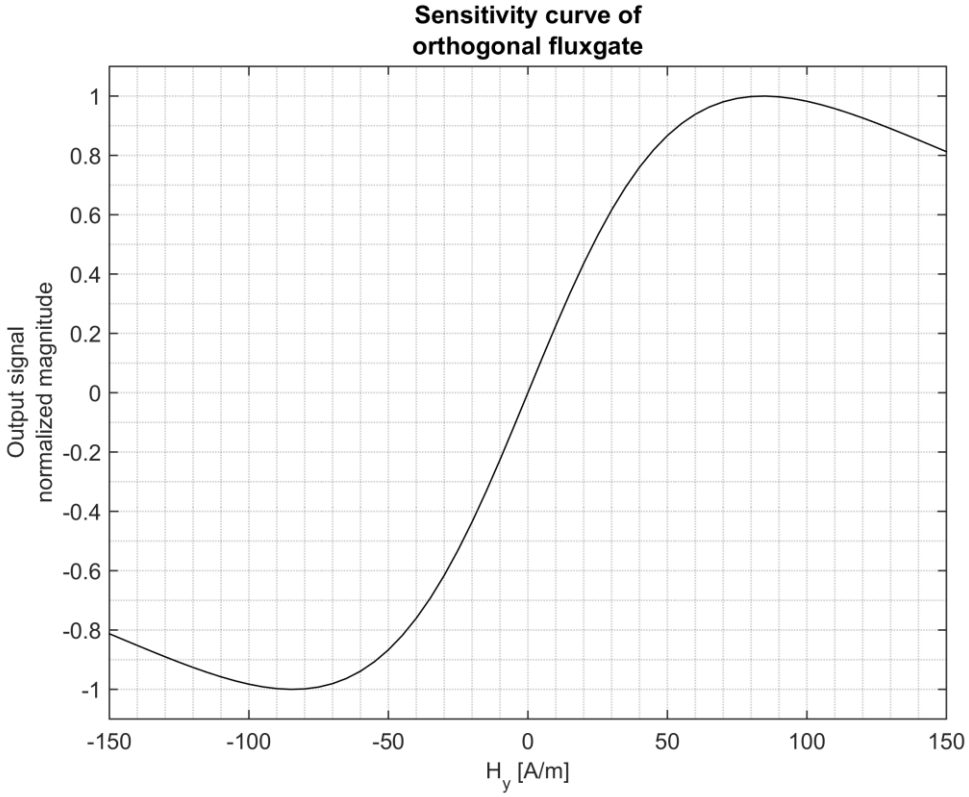

Figure 8: Sensitivity curve of orthogonal fluxgate in fundamental mode. The vertical axis represents normalized output voltage amplitude. The horizontal axis represents sensed magnetic field. Calculated using H_{EX} varying from 80 A/m to 185 A/m, core radius R = 60 μm. Here, the negative amplitude means signal with phase shift of π radians.

It is important to note that the voltage induced in the pickup coil is not generated purely from the rotation of magnetization vector. There is also component induced by time variations of present flux in the pick up coil, other than the flux due to magnetic core. By Faraday's law

$$V = \frac{\partial \phi}{\partial t}, \tag{13}$$

but its contribution to the output signal is basically negligible.

Up to now only isotropic ferromagnetic core has been considered. Anisotropy can have both positive and negative effect on the performance of the sensor depending on anisotropy direction. Consider the anisotropy that has component out of XZ-plane. It affects the field energy expression by adding one more term:

$$E_{tot} = -\mu_0 M(H_{DC} + H_{AC})\cos\alpha - \mu_0 M H_y \cos\left(\frac{\pi}{2} - \alpha\right) + \mathrm{k}\sin^2(\gamma - \alpha), \qquad (14)$$

where γ is angle of the anisotropy with respect to XZ-plane (cylindrical core cross-section) and k is anisotropy constant.

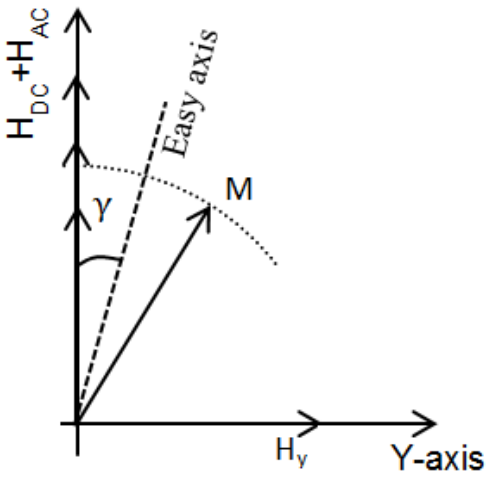

Figure 9: Angle of the anisotropy γ with respect to XZ-plane of the sensor core.

When $H_y = 0$ the energy term due to anisotropy will affect the angle α, creating a non-zero output signal. On the other hand, if the anisotropy is in the circumferential direction it will work in the same way as the DC bias to keep the wire saturated and therefore to reduce the noise [9].

2.3 Difficulties in operation

The offset introduced by axial anisotropy component causes several problems. If the offset was high, but stable, it would not affect the sensor performance, because if we precisely know its value then we can easily compensate it without loss of sensitivity. However, most frequently the offset is unstable in time and is also highly dependent on temperature. This introduces a large low-frequency noise which can be seen in Figure 10. The variations can be order of several nT over an hour.

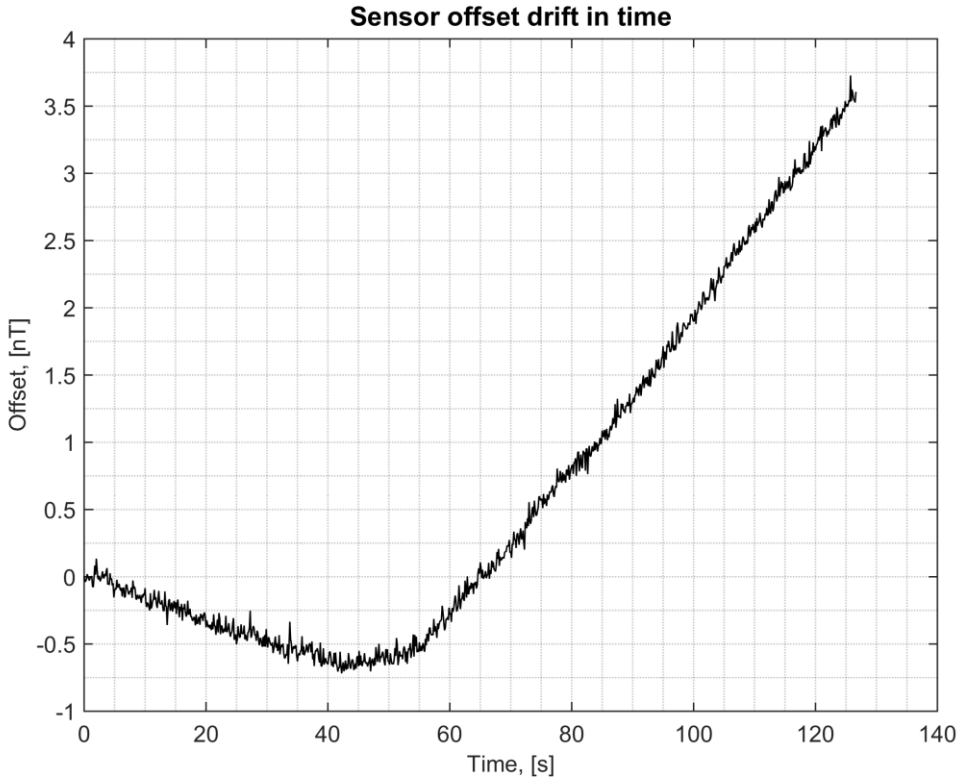

Figure 10: Offset drift in time. Figure obtained for positive bias current.

Figure 10 represents the output of the fluxgate sensor in 6-layer shielding. We excited the sensor using I_{DC}=50 mA, I_{AC}=40 mA at 100 kHz. We acquired the output voltage of the sensor with 1 MHz sampling frequency with 22 bit digitizer and we performed digital demodulation of the first harmonic.

II. Solutions

1. DC Bias Flipping

There is a simple way to suppress the offset caused by non-circular anisotropy: the method is based on periodically flipping of the DC bias polarity [10]. As a result the sensitivity is reversed, but the offset remains the unchanged. Then, the output signals obtained with each polarity are subtracted to obtain an offset-free characteristic. Figure 11 derived analytically represents the sensitivity curves of the sensor with positive DC bias, negative DC bias and after compensation is applied.

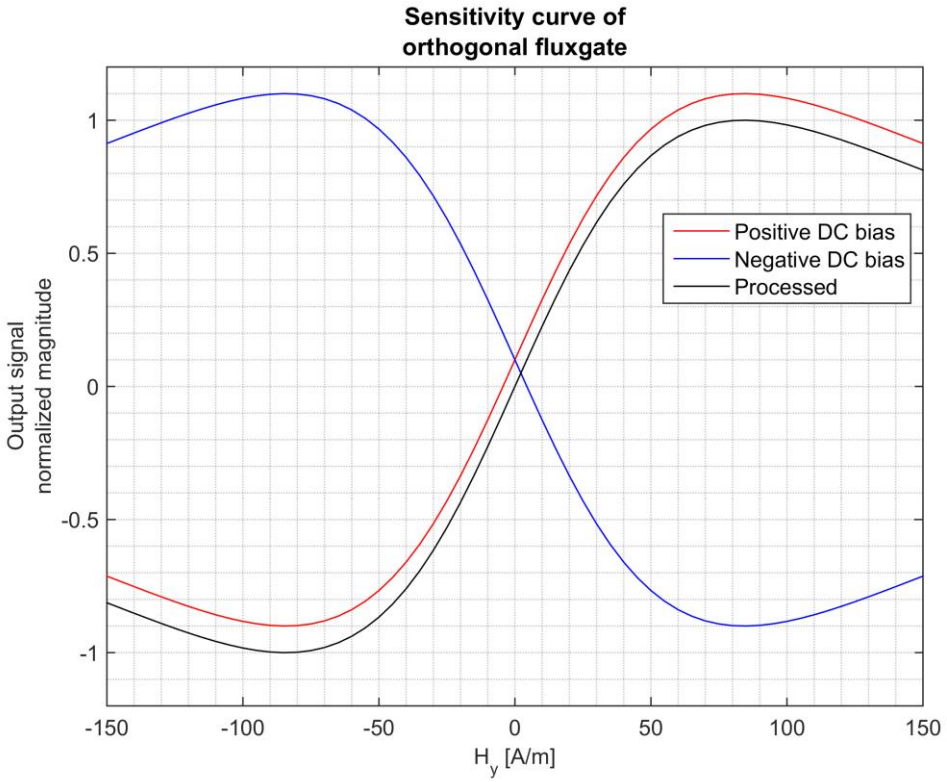

Figure 11: Sensitivity of fundamental mode orthogonal fluxgate for positive and negative DC bias current. The responses are calculated using H_{EX} varying from 80 A/m to 185 A/m, core radius R = 60 μm. Here the negative amplitude means signal with phase shift of π radians.

The reason of such behavior can be found in the working mechanism of the sensor. First let us analyze the reason why the sensitivity is reversed. Let us consider the AC

bias current to be a sine wave. The output signal for positive DC bias is shown in Figure 12:

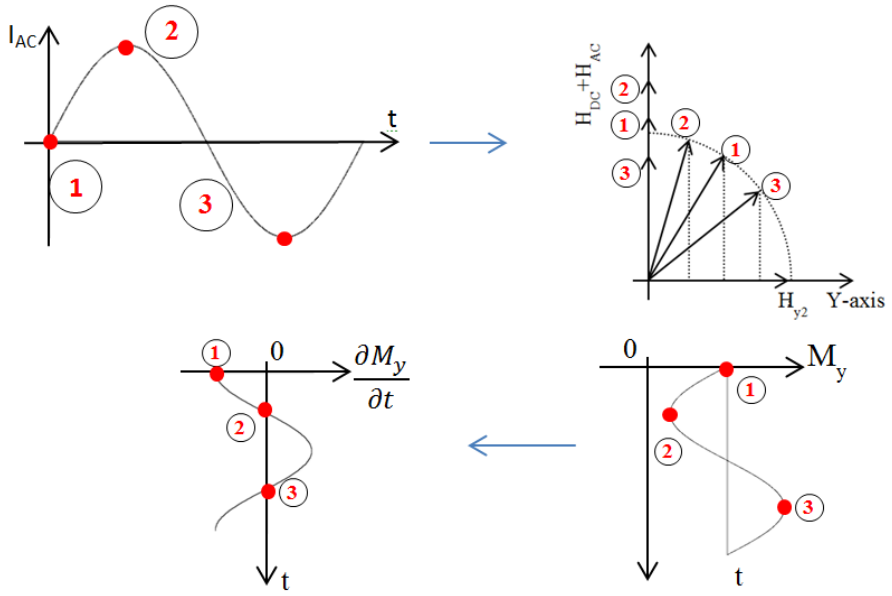

Figure 12: Output signal during positive DC bias.

Figure 13 shows the output signal during the negative polarity of the DC bias. It can be seen that the two signals have phase shift of π radians, which corresponds to reversed sensitivity on the sensitivity curve (Figure 11).

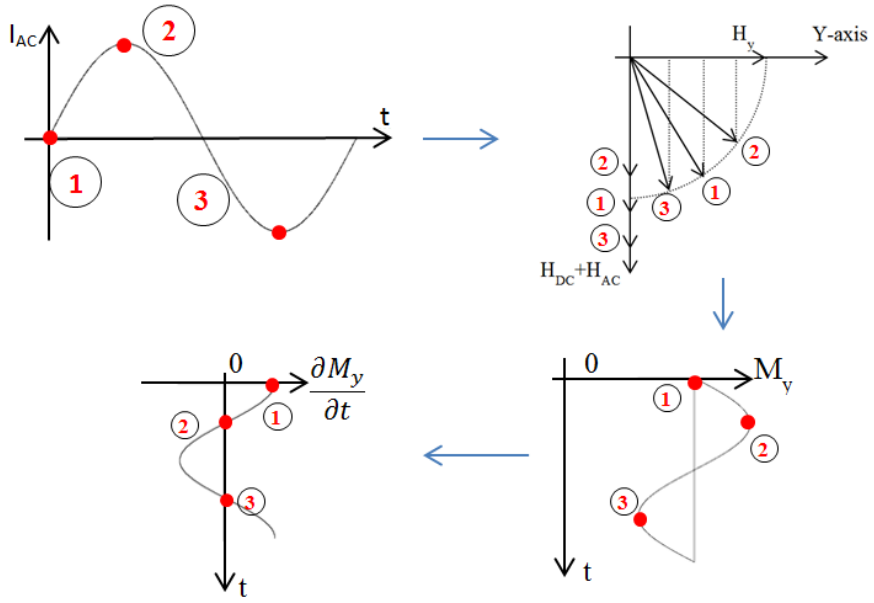

Figure 13: Output signal during negative DC bias.

While the sensitivity is reversed, the offset given by the non-circular anisotropy remains the same. Let us consider the sensor output signal when the core anisotropy has non-circular component and there is no H_y field. The output will be non-zero given by the anisotropy and it will have phase shift –π/2 radians with respect to excitation current. This can be seen in Figure 14.

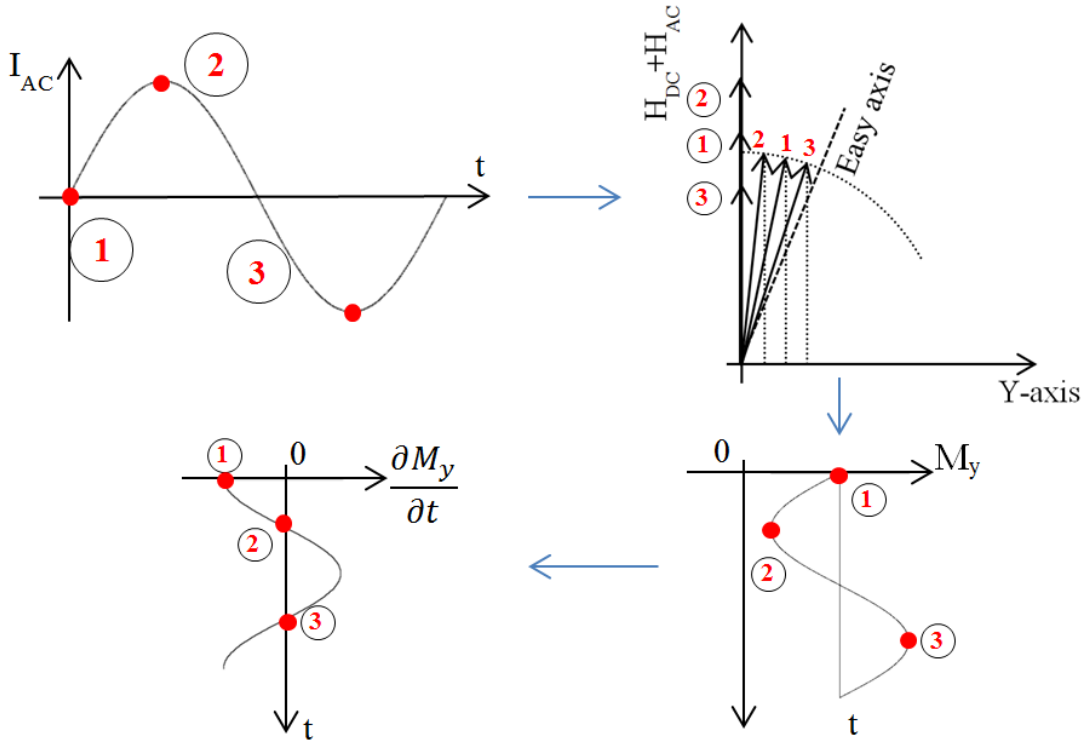

Figure 14: Sensor offset during positive DC bias.

Now consider the sensor output during negative DC bias, which is shown in Figure 15. The output signal has phase shift –π/2 radians with respect to excitation AC current as well. Hence, the offset sign does not change when we flip the DC bias only.

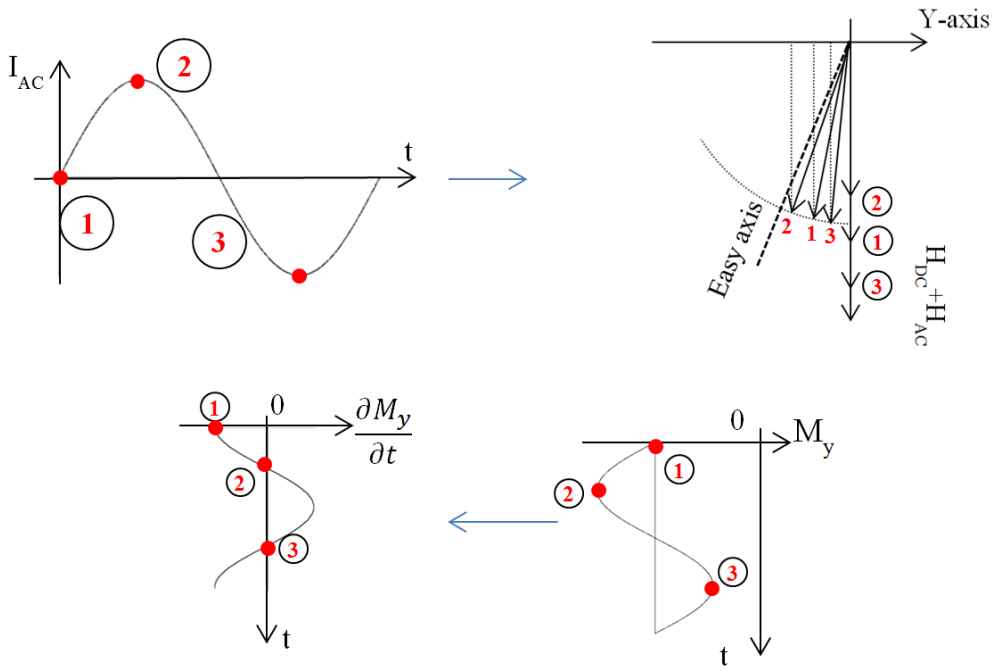

Figure 15: Sensor offset during negative DC bias.

For such operating mode we need to excite sensor with DC bias of the same magnitude, but opposite polarities. On practice this means that two voltage sources are required. This solution will introduce additional noise to the system, because voltage sources will have different operation characteristics, like temperature dependence, voltage variations in time and even voltages themselves may not be identical. All these imperfections are sources of additional noise.

A partial solution consists of using a single dc voltage source and inverting it by using a well-designed inverting amplifier; in this way any change of the voltage source at frequency lower than the switching frequency would be equal for both polarities. However, even with this method we cannot compensate the change of the offset voltage of the inverting amplifier in time.

2. Proposed solution

In order to overcome these issues we decided to use a different method. We do not switch the sign of the DC bias, instead we periodically flip the polarity of both I_{DC} and I_{AC}.

In this operating mode the offsets have different signs in positive and negative sensor polarity, but the sensitivity remains the same. Consider sensor operating in positive polarity exposed to a positive magnetic field H_y. As we have already mentioned, the output voltage induced in the coil is proportional to $\frac{\partial M_y}{\partial t}$. The mechanism leading to the output voltage for positive polarity of the magnetic wire is shown in Figure 16.

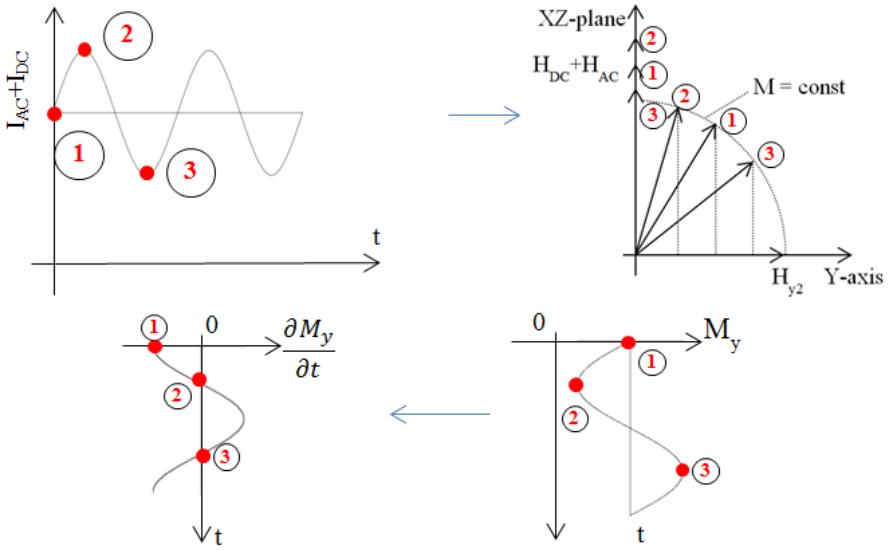

Figure 16: Output voltage of the sensor during positive polarity of the sensor.

On the other hand, the output voltage at negative polarity is generated according to the mechanism shown in Figure 17. We can see that for both polarities the output voltage has the same phase, hence the sensitivity is not reversed.

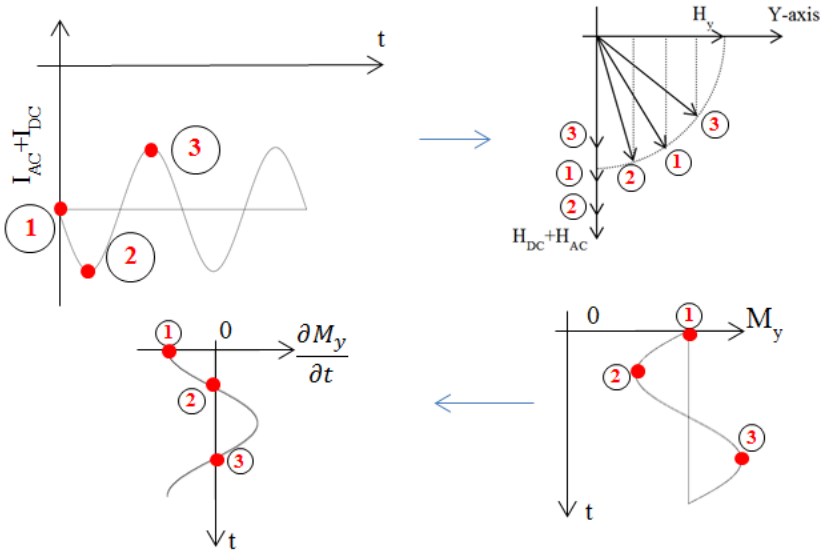

Figure 17: Output voltage of the sensor at negative polarity.

However, in case of non-circular anisotropy the offset is reversed by the polarity flipping. In Figure 18 we can see the output signal with no H_y field present during the positive polarity of the sensor.

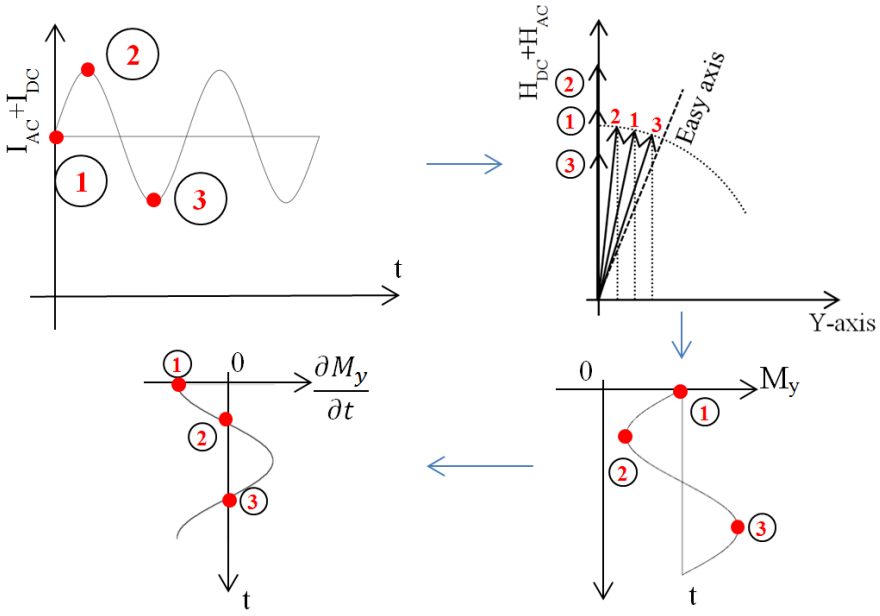

Figure 18: Sensor offset for positive polarity.

From comparison to the sensor offset signal during negative polarity (Figure 19) it can be seen that the two signals have phase shift π radians, which means the sign of the offset is reversed.

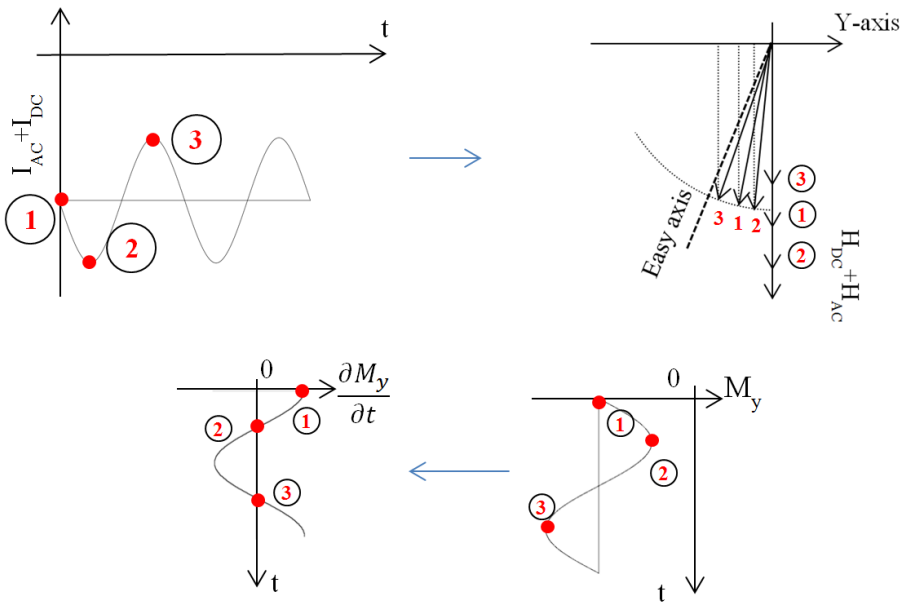

Figure 19: Sensor offset for negative polarity

The resulting characteristic with positive and negative polarity therefore will be as in Figure 20. It is sufficient to sum the values obtained with both polarities to have an offset-free characteristic.

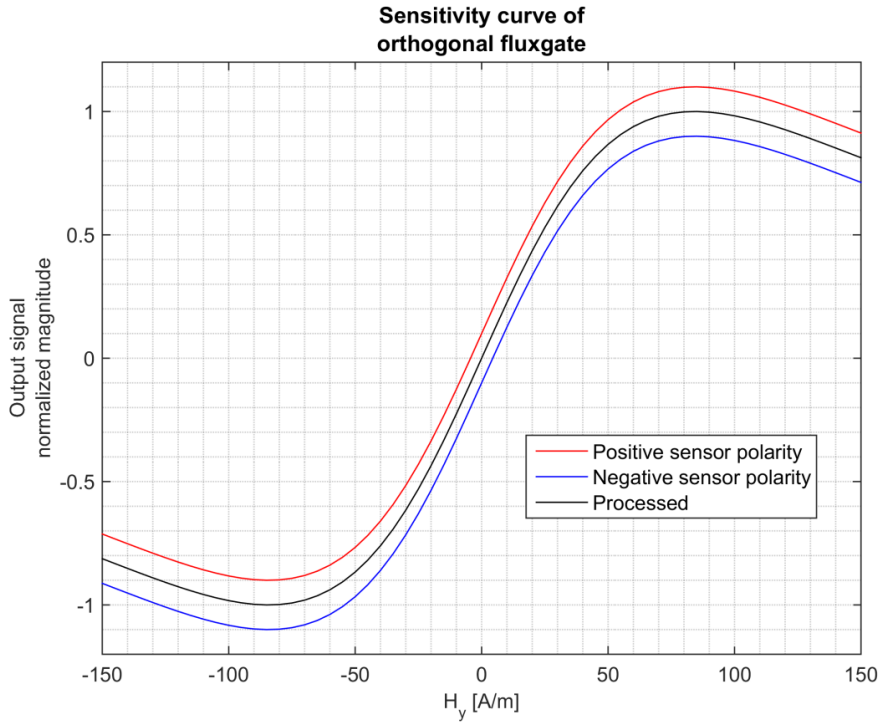

Figure 20: Sensitivity of fundamental mode orthogonal fluxgate for both polarities. It can be seen that offsets have the same magnitudes, but opposite signs. Calculated using H_{EX} varying from 80 A/m to 185 A/m, core radius R = 60 µm.

The advantage of this method is that it requires only one source for DC bias, therefore we do not have the need of two identical DC biases with opposite polarity. We periodically flip the polarity of the magnetic wire using solid state switches and inject the excitation current from opposite directions. This method is implemented by the schematic shown in Figure 21.

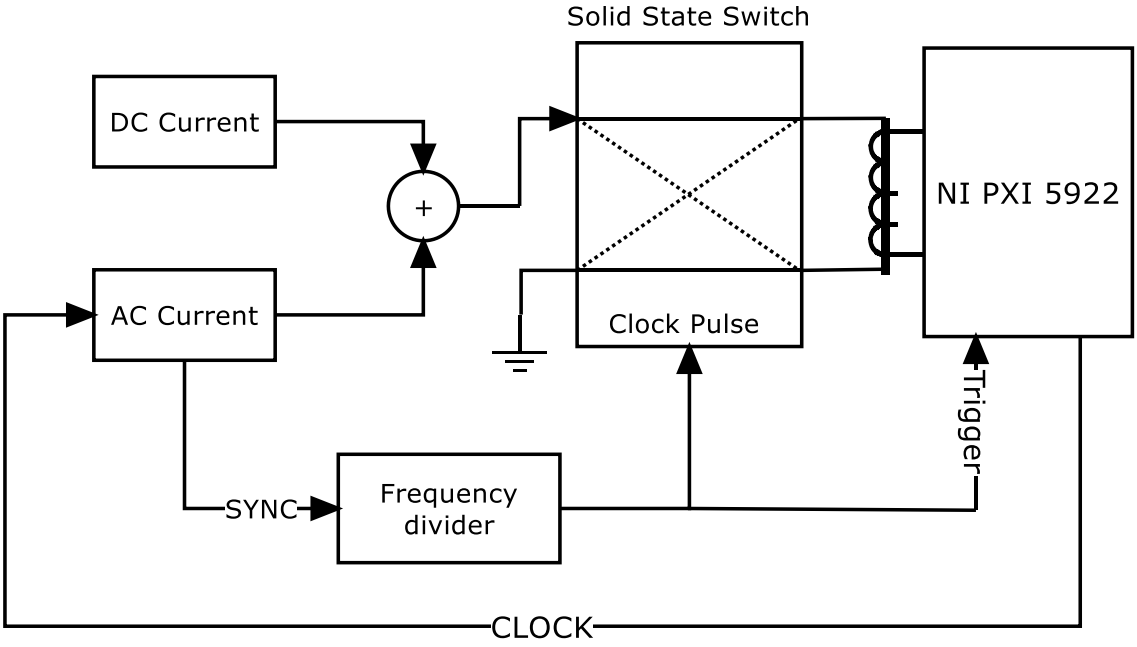

Figure 21: Schematic of the controlling electronics of the sensor.

The PCB of the used flipping circuit and the schematic can be found in Appendix A and Appendix B.

The excitation current is generated by the circuit shown in Figure 22. We use 12 V accumulator connected to a 7805 voltage stabilizer to generate the 5 V DC voltage source. The 5 V are connected to the sensor via 100 Ω resistor to generate 50 mA DC bias current. The 8 V peak-to-peak sine wave at 100 kHz from waveform generator connected to 100 Ω resistor and blocking capacitor 890 nF is used to form 80 mA peak-to-peak AC bias current. The excitation current is then periodically flipped by the solid state switches.

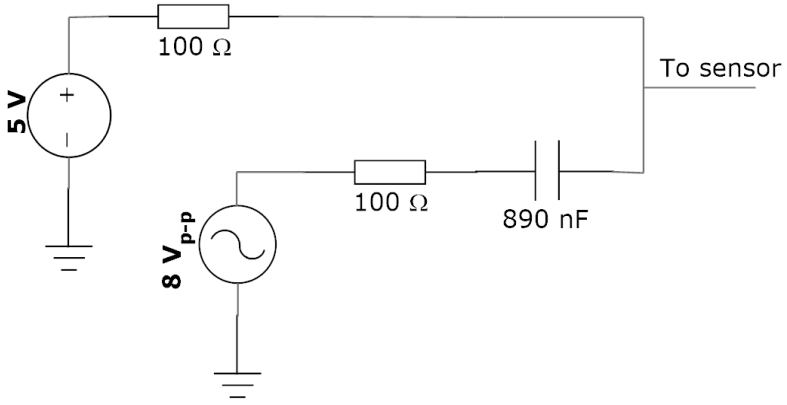

Figure 22: Excitation current generator schematical representation.

The sensor core is connected to the solid state switches by coaxial cable. In one polarity the central wire of the cable is used to inject the current and the shielding is used as the return wire, and in the opposite polarity it is vice versa. The pick-up coil is connected to the digitizer by a coaxial cable. One pin of the coil is connected to the central wire of the cable and the other is connected to the shielding.

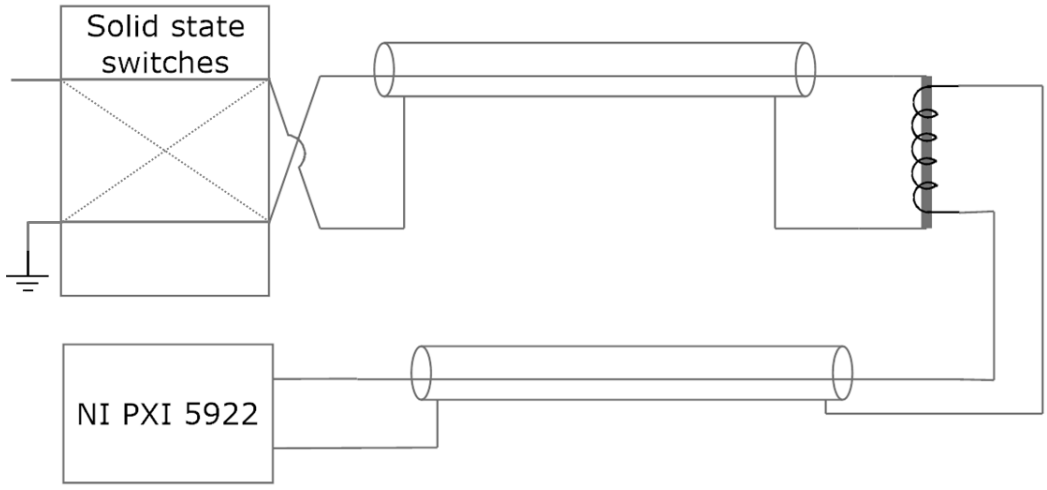

Figure 23: Schematic representation of connection of the sensor.

The SYNC TTL signal from the waveform generator is fed to frequency divider 74HC4040 and the signal from the divider is fed to NAND gate 74HCT00N to generate the two digital signal of opposite polarity used to control the solid state switches ADG452BNZ which flip the sensor polarity. The ADG452BNZ has $t_{on} = 70\,ns, t_{off} = 60\,ns$ – the switching time is small enough so that switch does not affect the transient

that we observe. The resistance of the channels is $R_{on} = 4\ \Omega$, and is small compared to resistance of other components. This means that change of the channel resistance will not significantly affect sensor response and can be neglected. The resistance match of the channels is $\Delta R_{on} = 0.1\ \Omega$, which means that the asymmetry between two paths of the excitation current is negligible and the two polarities of the sensor can be considered symmetric.

The output signal is obtained by digital demodulation of the voltage induced in the pick-up coil. We sample the sensor output voltage by National Instruments PXI 5922 at 1 MHz sampling frequency with 22 bit resolution over a 1 V voltage range. The voltage generator which provides the I_{AC} is locked to the digitizer by 10 MHz clock generated by the digitizer. In this way both the digitizer and the waveform generator share the same time base. For this reason we achieve a very good synchronization and we do not need to apply any window.

Each period of the voltage (100 kHz) is demodulated singularly. For each value of the 1st harmonic we extract the real part of the phasor. The reference phase is the phase of the excitation current reduced by a constant phase in order to maximize the sensitivity (see Paragraph III.1). In such way we obtain series of samples representing the real part of the voltage for each period. In most of the conducted experiments the frequency of the current was divided by 256, which means 128 samples are obtained for positive polarity and 128 for negative. The samples obtained for both polarities are then averaged.

The polarity switching that we use to operate the sensor introduces additional transients and noise to the sensor output. However this effect only lasts for the first few periods of the excitation AC current after the flipping. We eliminate it by disregarding first 50 periods of each polarity.

III. Results

1. Maximizing Sensitivity

In order to calculate the sensitivity of the sensor we subjected it to field from -10 A/m to +10 A/m in Helmholtz coil. The field was small enough not to exceed the linear region of the sensor. We excited the sensor with I_{DC}=50 mA, I_{AC}=40 mA at 100 kHz and we acquired the output voltage of the sensor with 1 MHz sampling frequency. We demodulated every single period of the output voltage singularly: in this way we obtain a series of 128 samples representing the real part of the voltage for positive polarity followed by 128 samples for the negative polarity. Then we took the average of the obtained two groups of samples. The resulting sensitivity versus reference phase graph is shown in Figure 24. The vertical axis represents sensor sensitivity in V/T, the horizontal axis represents phase reference in radians.

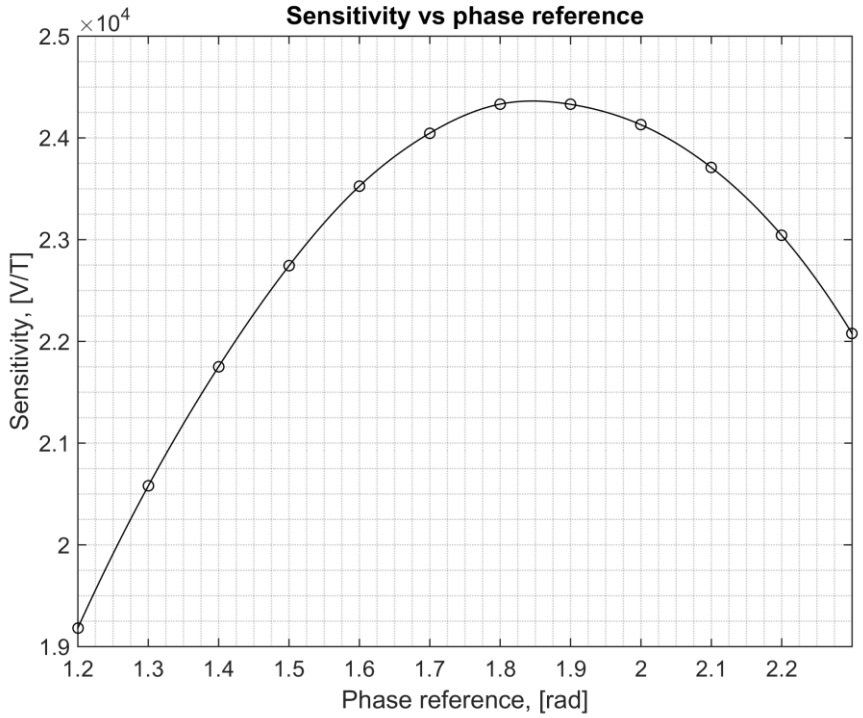

Figure 24: Dependence of sensor sensitivity on the reference phase.

In order to achieve maximal sensitivity it is necessary to set up the phase reference. In the further experiments reference phase of 1.8 radians was used. This allowed us to reach sensitivity of 24,330 V/T.

2. Dependence of transient on phase

A very important aspect of the proposed operation principle is switching phase, i.e. phase of excitation current waveform at which we perform sensor flipping.

Flipping the polarity of the sensor might create high overshoot due to transient of exponential shape, which is caused by quick change of saturation polarity of magnetic wire. This overshoot by itself can be a source of additional noise. Its magnitude and shape highly depend on the switching phase (Figure 25). By switching phase here I refer to phase of the excitation AC current at which the flipping occurs. If the transient is different from period to period it is source of additional noise. Hence in order to minimize the noise it is necessary to always flip the sensor polarity at the same phase of excitation current. This means that it is necessary to synchronize the excitation current of the sensor with the switching control signal. This is achieved by feeding the sync TTL signal to frequency divider and then using it to flip the sensor.

In order to check this theory we conducted a following experiment. We excited the sensor with I_{AC} = 80 mA peak-to-peak generated by Rigol DG1062 waveform generator connected to 100 Ω resistor. This generator has two channels and we are able to adjust the phase between excitation current and switching signal. The frequency of excitation current was 100 kHz, the frequency of the switching signal was 1562.5 Hz i.e. we measured 64 periods per switching period – 32 corresponding to positive polarity and 32 to negative. The DC excitation current was I_{DC} = 50 mA. The output signal was then acquired by PXI at 1 MHz sampling frequency.

Figure 25 represents the dependence of overshoot magnitude on switching phase. As a reference value we took the maximal absolute value of output signal acquired and demodulated by the digitizer. We can see that the highest overshoot occurs at 150°-180° switching phase. The typical shape of the output at these conditions can also be seen at the graph. The lowest overshoot occurs at 50°-100° and 250°-290° switching phases and the typical transient shape can be observed in Figure 25 as well.

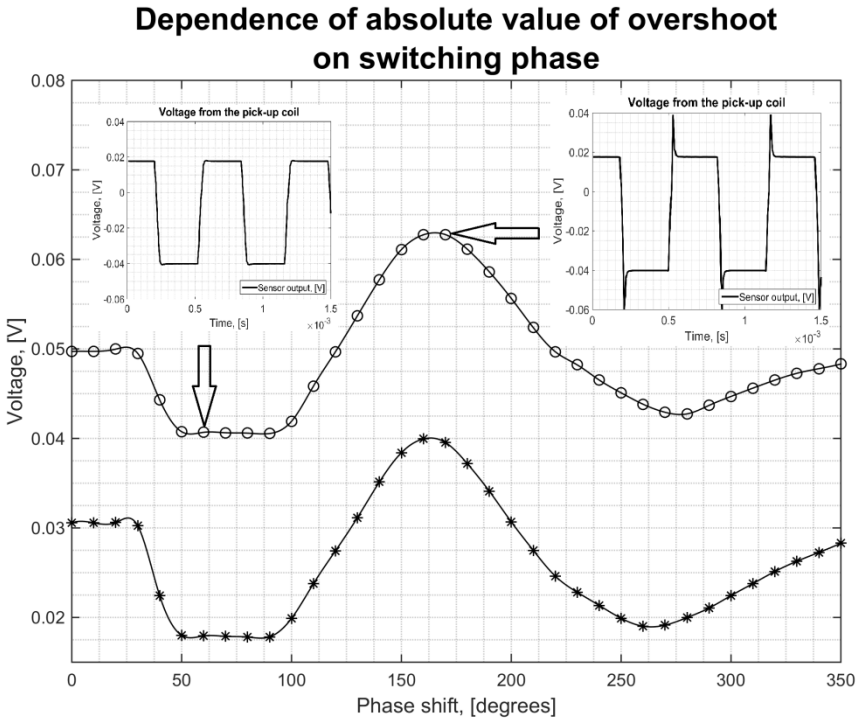

Figure 25: Dependence of the overshoot value and transient shape on switching phase.

This result proves that it is indeed important to keep the switching phase constant because transient shape highly depends on the switching phase, and it confirms the necessity of synchronizing switching signal to excitation current waveform. If the switching was not synchronous with the excitation current, every time the switching would occur at different phase of the excitation current, resulting in different transients. The effect of transients on sensor performance will be further analyzed in chapter 4.

3. Transient stability

In the previous chapter we have derived the importance of keeping the switching phase constant over time, in order to keep the shape of the transient constant to reduce the noise. In this chapter we will examine if it is necessary to use switching phase with low absolute value of overshoot.

The noise floor and the sensitivity are influenced by the number of samples per flipping period that can be used to extract the measured magnetic field, because statistically uncorrelated noise decreases as the square root of the number of samples averaged. Intuitively it may seem that periods during the transient cannot be used, because we must wait the transient to be finished. From this point of view it might seem necessary to select the switching phase which gives the lowest overshoot, because the higher the overshoot the longer is the time it takes to stabilize.

In order to examine this theory we analyzed the data obtained from the sensor. We excited it with I_{DC} = 50 mA, I_{AC}=40 mA at 100 kHz and we acquired the output voltage of the sensor with 1 MHz sampling frequency. We set the switching phase to 60°. The signal was processed in the same way as described in the previous chapters with 1562.5 Hz switching signal resulting in 32 samples for each sensor polarity. We acquired the signal for 0.064 seconds which gave us 6400 samples or 100 flipping periods to analyze. From each period we extracted the part corresponding to positive polarity of the sensor (samples 30-64). Based on this data we calculated average shape of the output during positive polarity. Finally, we subtracted the average shape from each of the 100 periods. The obtained result can be seen in Figure 26.

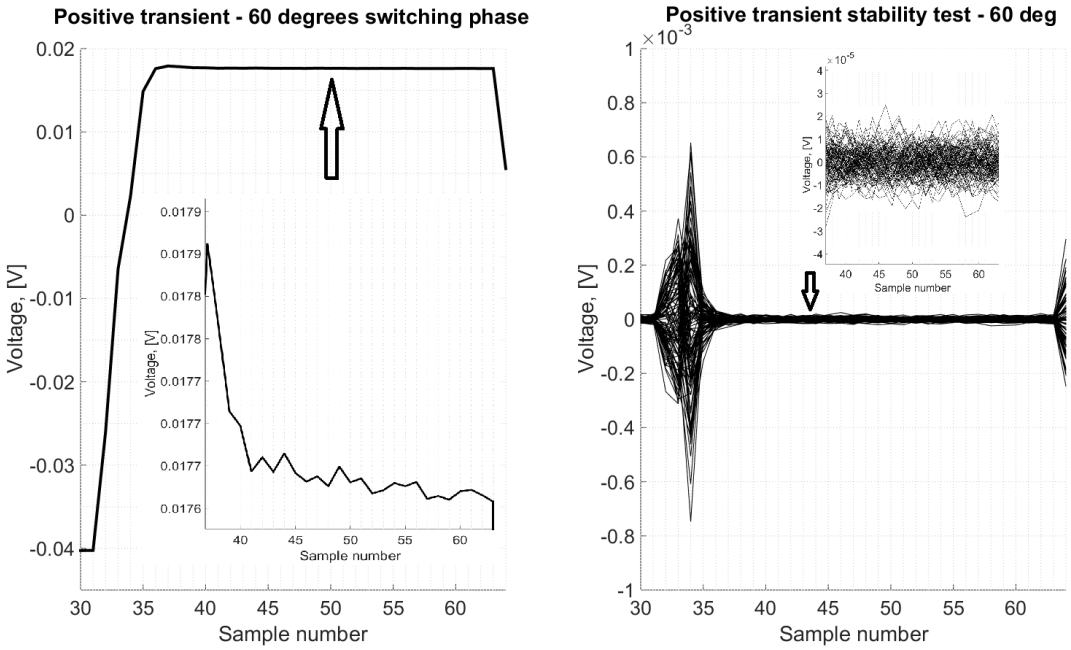

Figure 26: Positive transient at 60° switching phase (left) and deviation of transients from the average shape (right).

We can see that the exponential transient in fact lasts until next switching. However, we observed that the shape of the transients remains relatively constant from period to period. At the beginning and at the end there are some samples that have a large deviation of 1 mV peak-to-peak, but then it gradually reduces to only 40 μV, which is 25 times less. This result means that if we exclude these noisy samples from calculation of magnetic field then we expect not to increase the sensor noise.

We have repeated the same procedure for 160° switching phase, because at this condition we observed a high overshoot. The result can be observed in Figure 27. Analysis has revealed the same convergent behavior of the large transient. Moreover, the number of "noisy" samples does not increase. This result is of a particular interest because it means we can use any phase for flipping the sensor polarity. It is only important to keep it constant over time.

In order to further check this result we conducted the following experiment. The excitation current remained as described at the beginning of this chapter. We have decreased flipping signal frequency to 390.625 Hz in order to obtain 256 samples per flipping period or 128 samples of positive polarity and 128 of negative.

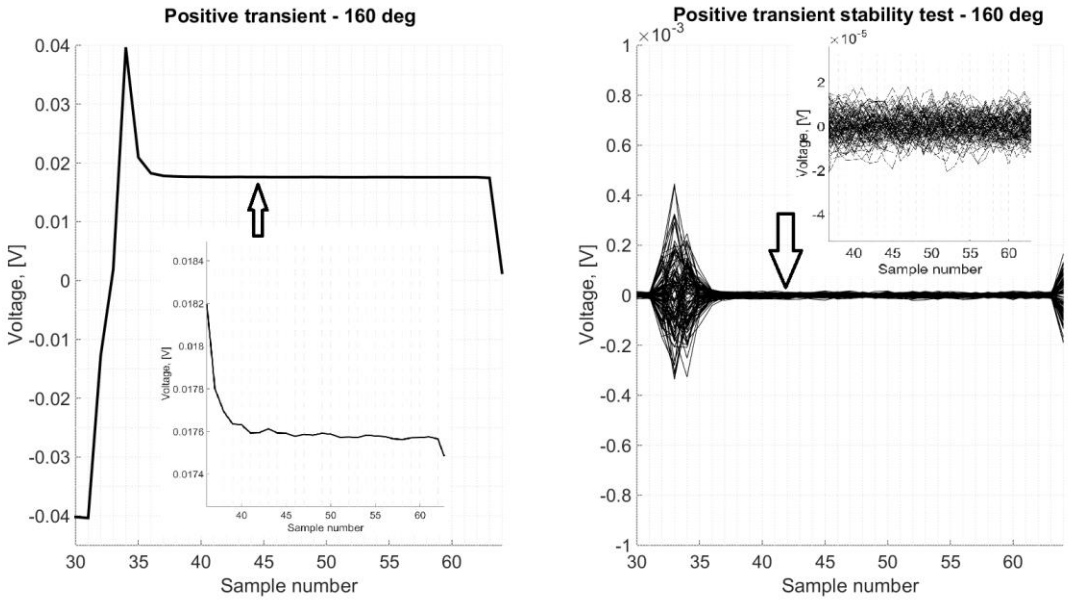

Figure 27: Positive transient at 160° switching phase (left) and deviation of transients from the average shape (right).

We placed the sensor inside 6-layer shielding and measured the noise by acquiring 768000 samples (or 3000 flipping periods) during 7.68 seconds. The output signal was obtained by calculating the average of 5 periods selected at different delay from the switching moment in order to analyze the level of noise of the output signal in different position after the flipping. If what we have explained before is correct we expect to see high noise level for the first periods after flipping, while the noise rapidly drops for the following periods due to a persistent shape of the transient. We started by taking periods from 1st to 5th (after the flipping) of the positive polarity, then we considered the periods 6th to 10th, 11th to 15th and so on. The samples used for calculation are represented on the horizontal axis of Figure 28.

We considered the noise floor of the obtained noise spectrum as the reference value. The vertical axis of Figure 28 represents it. We can see that the noise of the first five periods is 30 $\frac{\mathrm{pT}}{\sqrt{\mathrm{Hz}}}$ and is the highest among the reviewed parts of the period. The noise rapidly decreases as we move towards the central samples of the period, with only 1.6 $\frac{\mathrm{pT}}{\sqrt{\mathrm{Hz}}}$ in periods 6th to 10th and 1.5 $\frac{\mathrm{pT}}{\sqrt{\mathrm{Hz}}}$ in periods 10th to 14th.

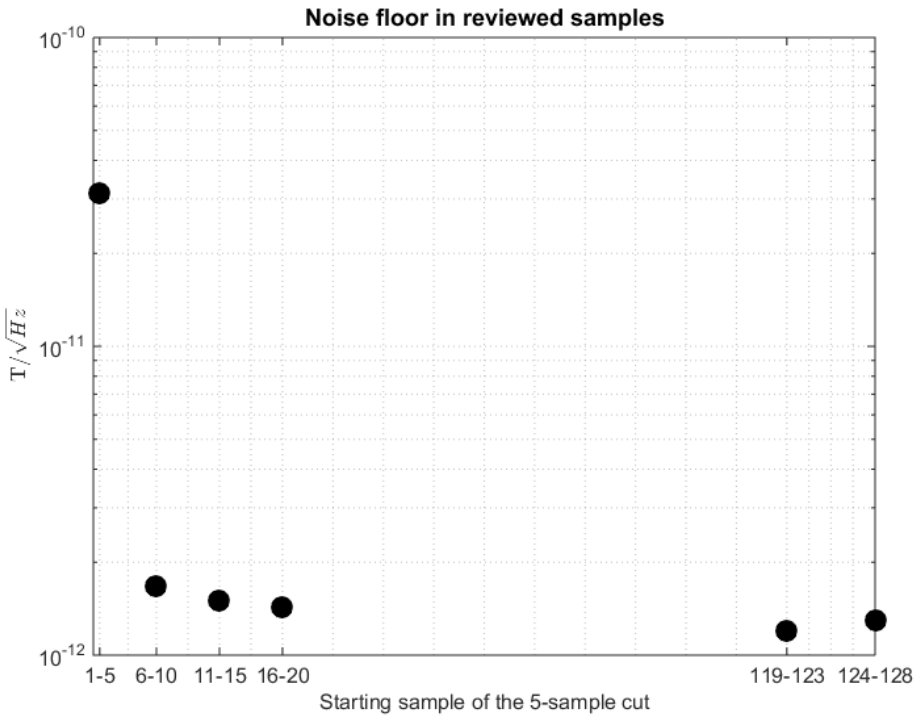

Figure 28: Noise level in different parts of the switching period.

This result proves that indeed only first few periods after the switching are noisy. It is important to mention that the final noise floor will be smaller than shown in Figure 28. This is given by statistical averaging of the noise, which is more effective the larger the number of samples is used. This is why it is important to find a compromise between cutting the noisy periods and the need to use more periods for noise reduction.

4. Noise comparison

In order to test the performance of the resulting system we conducted the following experiment. The excitation current remained as in the chapter 3, namely I_{DC} = 50 mA, I_{AC}=40 mA at 100 kHz. The frequency of the flipping signal was 390.625 Hz such that we had 256 samples per switching period, 128 during positive polarity and 128 during negative polarity.

Before starting the experiment we set the reference phase 1.9 radians corresponding to largest sensitivity of 24,330 V/T. Then we put the sensor inside 6-layer shielding. We acquired 768000 samples during 7.68 seconds, or 3000 flipping periods. We cut first 50 and last 9 samples from each polarity and based on this data we calculated the spectrum of magnetic field as measured by the sensor. The spectrum of our system averaged 20 times and the spectrum of the same sensor without flipping can be observed in Figure 29.

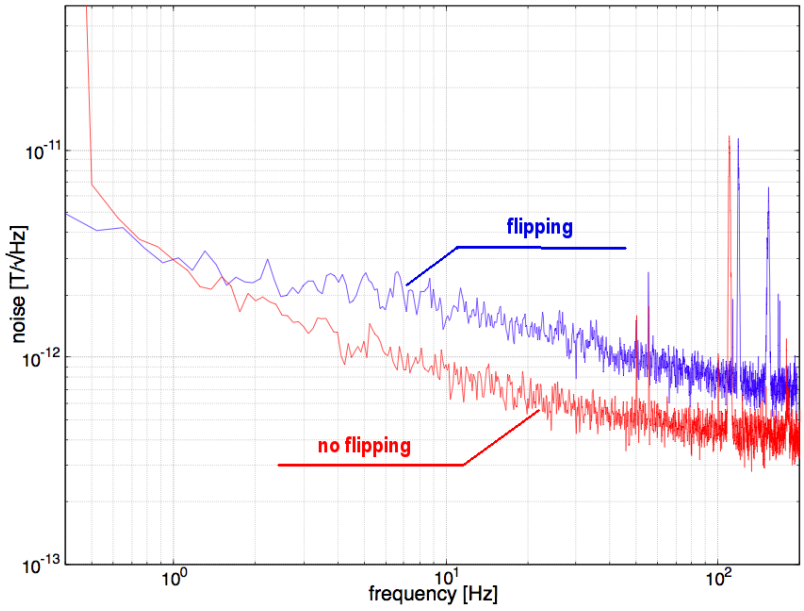

Figure 29: Spectrum of flipped and non-flipped fundamental mode orthogonal fluxgate. The red line corresponds to fluxgate without flipping. The blue line shows spectrum of our system.

The red line corresponds to spectrum of orthogonal fluxgate without flipping and the blue line corresponds to our system with flipping operating at conditions described at the beginning of this chapter. It can be seen from the image that our system increases the noise floor only by 0.4 pT/$\sqrt{\text{Hz}}$. However we manage to suppress large low-frequency noise given by offset instability, which will be further discussed in chapter 6 and 7.

5. Offset stability in time

It was mentioned before that one of the effects of anisotropy in ferromagnetic core of the orthogonal fluxgate is appearance of offset. If the sensor is perfectly shielded it will still give output corresponding to some non-zero measured field. This effect can also be seen at the sensitivity curves in Figure 20. On the image below the offset is order of μT.

A perfectly constant offset could be easily compensated by taking it into account with calibration and will not be source of additional noise. However, if it is too large it could cause saturation of electronics. But what is more important is that the offset is unstable: it changes in time and it is temperature-sensitive.

In order to examine the achieved offset stability in time we conducted the following experiment. We operated the sensor under the conditions as described in chapters 4 and 5. The sensor was located inside a 6-layer shielding. The ambient temperature was kept as constant as possible and the driving electronic circuit was thermally insulated. We have measured the offset during 3 hours. Figure 30 shows the results of conducted experiment.

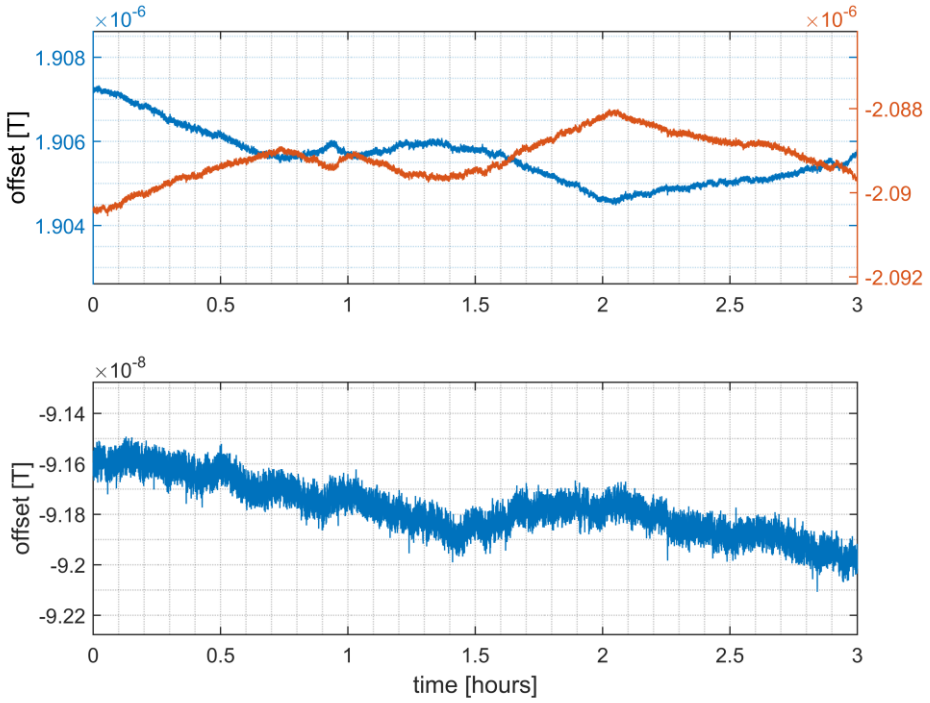

Figure 30: (Top) Sensor offset behavior in time if both polarities are processed separately. Blue curve corresponds to positive polarity, red curve corresponds to negative polarity of the sensor. (Bottom) Sensor offset behavior after averaging polarities

In Figure 30 you can see the offset behavior during the three-hour test. The blue line corresponds to positive polarity of the sensor and the red line corresponds to negative polarity. The measured difference between maximal and minimal value of the offset is 2.85 nT for positive polarity and 2.55 nT for negative polarity. After the compensation has been applied and the two polarities were averaged this offset drift was reduced to 0.62 nT during three hours. This is a significant improvement of sensor performance.

6. Offset stability with varying temperature

A very important aspect of sensor performance is temperature stability of the offset. Offset dependence on core temperature arises from the fact that offset is caused by axial anisotropy of ferromagnetic core.

Sensor is generally operated at different temperatures and we want the offset to be as constant as possible in order to provide a good compensation for it. The core anisotropy is expected to be symmetric in both positive and negative polarity providing symmetric offset variations. We expect that taking average of samples obtained for positive and negative polarity will not only suppress the voltage but also its thermal drift.

In order to verify this theory we conducted an experiment. The operation parameters of the system remained as described in chapter 4. Sensor was put inside a chamber where we could change the temperature; this chamber is located in a thermally insulated shielding, so that the sensor is shielded while the temperature of the shielding is not changing, thus providing constant remanence of the shielding magnetization. The distance to the bottom of the shielding was approximately 1/3 of its height provided that at this condition best shielding ratio is reached. Temperature inside the shielding was measured by PT-100 in 4-wires connection.

First we cooled down the sensor to -15 °C and let it warm up during 7 hours to +7 °C. The result can be observed in Figure 31. Offset drift of the positive and negative polarities treated separately was approximately 1.5 nT/°C. After the polarities were averaged the offset drift was reduced to 0.17 nT/°C.

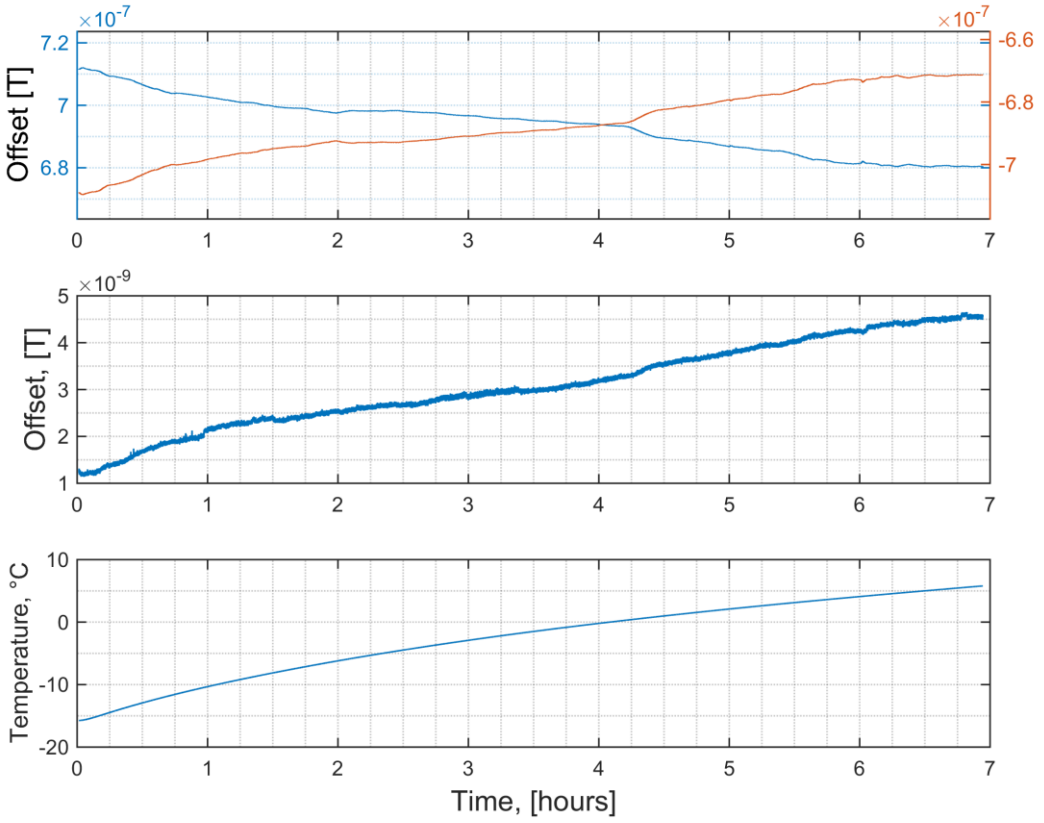

Figure 31: Offset thermal drift test results. (Top) Blue line corresponds to positive polarity of the sensor, red line corresponds to negative polarity. (Middle) Offset behavior after averaging the polarities (Bottom) Temperature during the test

Even if most of the thermal drift of the offset is suppressed, the resulting offset still drifts. However, it can be observed in Figure 31 that offset after compensation always drifts in the same direction as the offset of negative polarity. If we calibrate the sensor by multiplying the negative polarity periods by k=0.86 before averaging the polarities, thus calculating the output signal as $V = \frac{V_A + 0.86 \cdot V_B}{2}$ then the offset drift is almost totally suppressed, as seen in Figure 32. We obtain a maximum variation of 1.13 nT over a temperature range of 23 °C corresponding to 0.05 nT/°C. Clearly there is some asymmetry in the tested system.

One of the reasons may be different sensitivity in positive and in negative polarity. We have measured both as described in chapter 2 and the sensitivities differ not more than by 0.5%. Asymmetry in connecting wires could also cause 14% difference as they may react differently on the temperature changes.

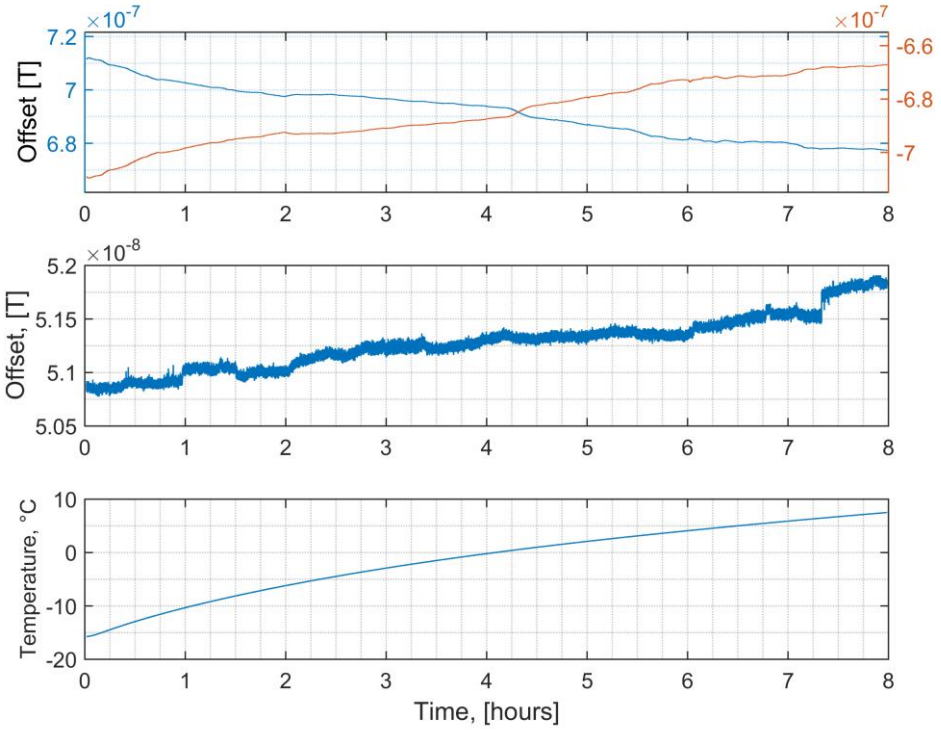

Figure 32: Offset drift test results after compensation was applied.

We managed to achieve a more symmetric behavior by connecting the core and the pick-up coil to the digitizer using differential connection with double core coaxial cables. The schematic of the connection is shown in Figure 33.

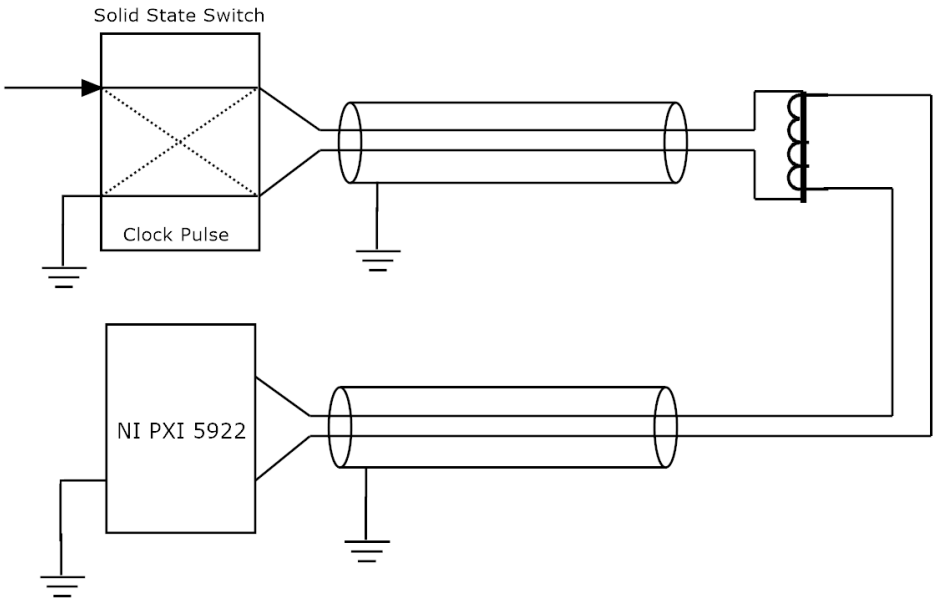

Figure 33: Schematic representation of connection of the sensor using double core coaxial cables with grounded shielding.

The current is injected into the sensor through one core of the coaxial cable and the other core is used as return wire. The shielding is connected to ground. Pins of the pick-up coil are connected through the cores of the coaxial cable to the digitizer in differential connection.

We repeated the same experiment as described earlier in this chapter. We have cooled the sensor from +16.5 °C to -15.5 °C during 1 hour and then we let it warm up slowly to +6 °C during 5 hours. We used the compensating coefficient k = 0.981 to calculate the output signal. The achieved results are presented in Figure 34.

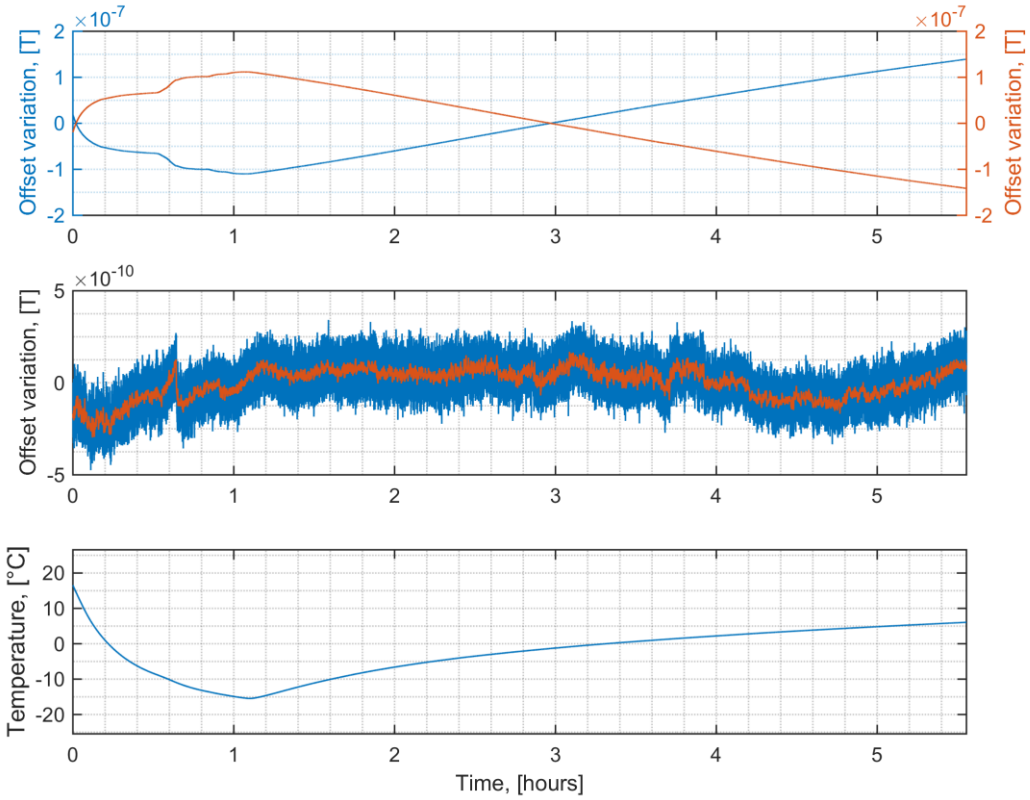

Figure 34: (Top) Offset thermal drift: blue line corresponds to positive polarity, red line corresponds to negative polarity. (Middle) Offset thermal drift after averaging polarities and applying compensation (blue line) and filtered output (red line). (Bottom) Temperature of the sensor

In Figure 34 (top) it can be seen that the thermal drift of the offset of both polarities during the conducted experiment was 200 nT. After averaging the two polarities and applying the compensation (Figure 34, middle) the offset variation was 0.5 nT over a temperature range of 32 °C corresponding to 0.016 nT/°C.

In order to test the sensor performance in the maximal available range of temperatures we performed another experiment. The experimental setup remained as described earlier in this chapter; the sensor was cooled from +54 °C to -17 °C during 12 hours. The sensor offset was recorded during this time (Figure 35).

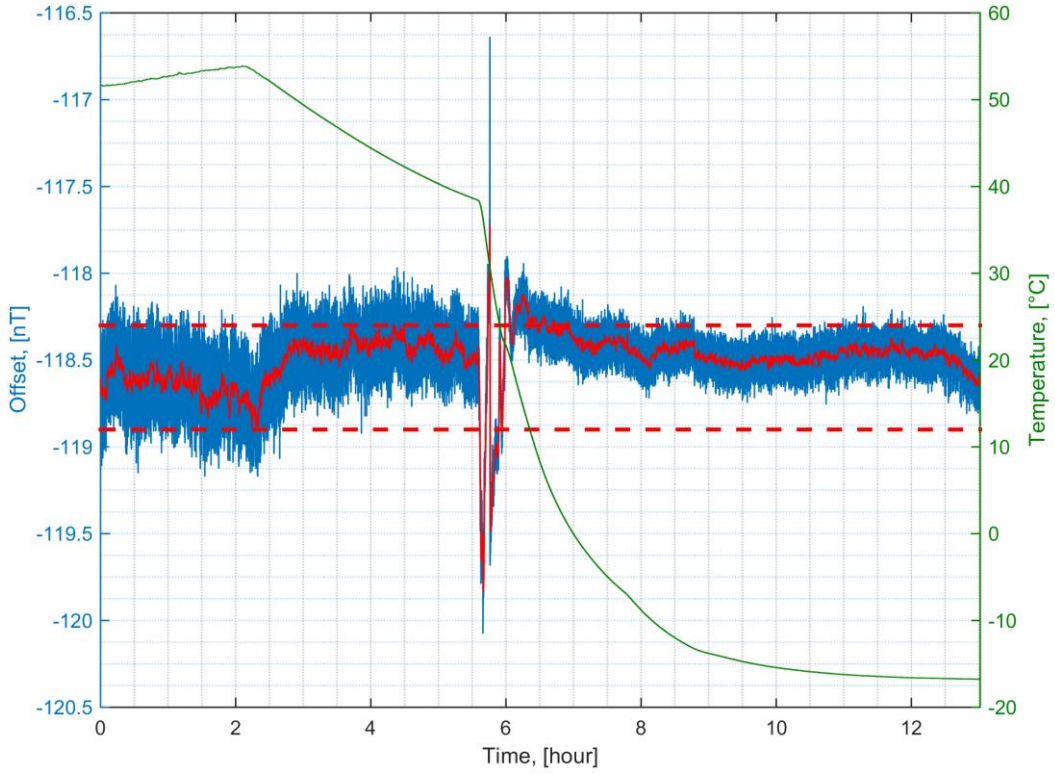

Figure 35: Fluxgate offset thermal stability test. Blue line corresponds to the offset (2 samples per second), red line is the sensor offset after filtering (moving average of 60 samples), green line is the temperature inside the shielding. The red horizontal lines correspond to a range of 0.6 nT

In Figure 35 it can be seen that the compensated offset drifts within 0.6 nT over 70 °C temperature range, resulting in thermal drift < 0.01 $\frac{nT}{°C}$. The sensor is however sensitive to quick variations of temperature. This can be seen in the large offset variation which occurs at around 5.5 hours from the beginning of the experiment.

However, this problem can be overcame by limiting the speed of temperature variation. An example is given in Figure 36 where we repeated the experiment by warming up the sensor in a similar temperature range. In this case we paid particular attention in avoiding rapid change of temperature: as we can see the offset was basically stable in

the whole temperature range (excluding a minor variation at the beginning of the experiment where we couldn't control the speed of variation of temperature).

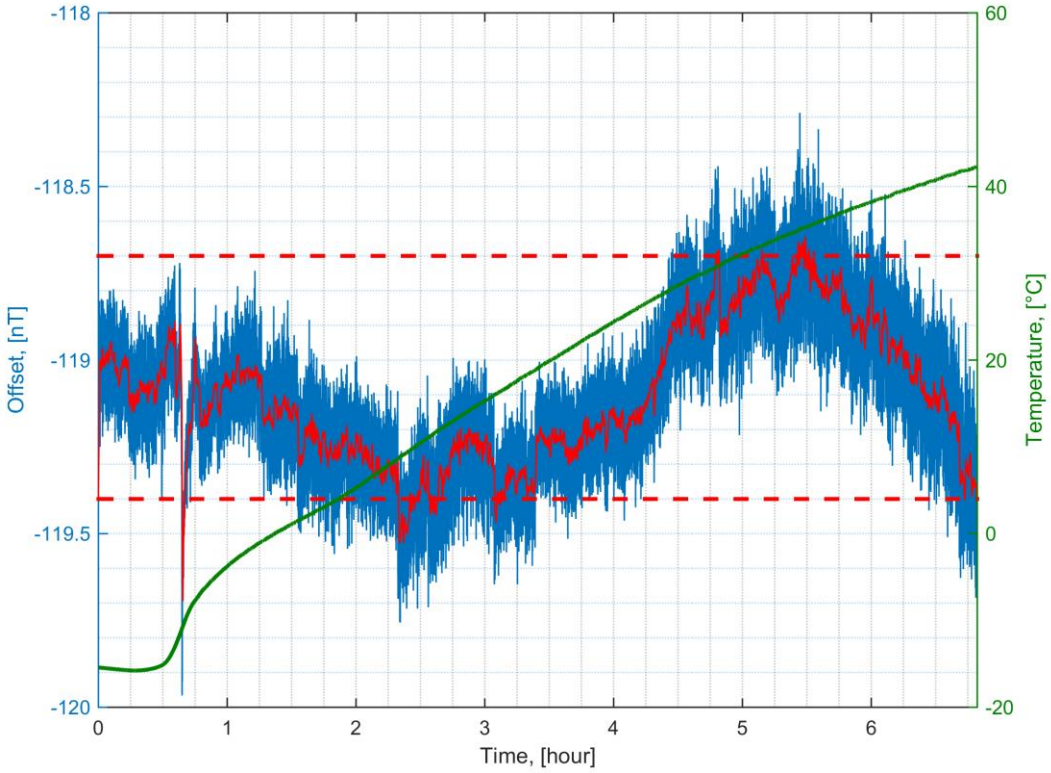

Figure 36: Fluxgate offset thermal stability test. Blue line corresponds to the offset (2 samples per second), red line is the sensor offset after filtering (moving average of 60 samples), green line is the temperature inside the shielding. The red horizontal lines correspond to a range of 0.7 nT

In this experiment the offset drift was 0.7 nT over 58 °C temperature range, resulting in thermal drift 0.012 nT/°C. The comparison of the achieved sensor offset thermal stability with other fluxgates is provided in Table 1.

	Thermal drift	Temperature range
Our system	< 0.015 nT/°C	-17 to +54 °C
Bartington Inst, U.K., **MAG-03** [11]	± 0.1 nT/°C	-40 to +70 °C
Stefan Mayer Inst, Germany, **FL1-100** [12]	< 0.1 nT/°C	0 to +70 °C
LEMI, Ukraine, **LEMI-022** [13]	< 0.5 nT/°C	-20 to +50 °C
Billingsley Aerospace and Defence, U.K., **TFM100G2** [14]	0.6 nT/°C	-55 to +85 °C
Y. Nishio et al [15]	< 0.02 nT/°C	-160 to +200 °C
	< 0.03 nT/°C	-160 to +200 °C
A. Cerman et al [16]	< 0.007 nT/°C	-10 to +60 °C
F. Primdahl et al [17]	< 0.008 nT/°C	-18 to +63 °C

Table 1: Comparison of the proposed system offset thermal stability with other fluxgates

The offset stability is one of the best among existing fluxgates. Moreover we achieved this result using cheap fluxgate with low excitation current and low power consumption and we do not have the necessity of expensive electronics.

IV. Conclusions

In this thesis I have described the proposed method of operation of orthogonal fluxgate in fundamental mode. I have briefly reviewed two of the most common magnetometers, explained the physical principle of fluxgate operated in fundamental mode, its set of problems and a used solution for overcoming these issues. I have then described the proposed system in details.

We flipped the polarity of both DC and AC excitation currents in order to suppress fluxgate offset time and thermal instabilities that result in large low-frequency noise. I have described the principle of the solution, the new problems that it causes and how to overcome these problems. We used solid state switches synchronized to the excitation current waveform and we investigated the importance of the synchronization. I have described the circuit that we developed and provided its schematics and PCB. I have then outlined the results of the performance tests of the proposed solution. We have managed to achieve offset thermal drift of < 0.015 nT/°C while increasing the high-frequency noise by 0.4 pT/$\sqrt{\text{Hz}}$ which is a tolerable amount. Such combination of characteristics has never been achieved on a cheap fluxgate sensor so far. Moreover, we have low power consumption because we use low excitation current below 100 mA and there is no need for expensive electronics.

During the tests we have observed unexpected asymmetric behavior of the fluxgate in positive and negative polarity, which we had to compensate. One of the possible future developments can be investigation of the physical nature of this asymmetry and its elimination. Substituting the voltage source connected to 100 Ω resistor by a current source could also improve the performance of the system. Another possible extension is development of portable excitation unit based on DDS microchip (AD9850, for instance) that is able to generate a current sine wave for excitation and a TTL square signal with adjustable phase shift with respect to current waveform to control the flipping.

v. References

[1] Tumanski, S.; Induction coil sensors – a review. *Measurement Science and Technology*, Vol. 18, Number 3, 2007, pp. R31–R46

[2] Gallop, J. C. & Petley B. W.; SQUIDS and their applications. *Journal of Physics E: Scientific Instruments*, Vol. 9, 1976, pp. 417-429

[3] Xie, M., Schneiderman, J.F., Chukharkin, M.L. et al.; High-Tc SQUID vs. low-Tc SQUID-based recordings on a head phantom: Benchmarking for magnetoencephalography. *IEEE Transactions On Applied Superconductivity,* Vol. 25, No. 3, June 2015, DOI: 10.1109/TASC.2014.2366420

[4] Butta, M.; Orthogonal Fluxgates. *Magnetic Sensors: Principles and Applications*, Chapter 2, Edited by K. Kuang, 2012, pp. 19-44

[5] Jiles, D.; *Introduction to magnetism and magnetic materials, ch. 6: Magnetic domains*. London: Chapman and Hall, 1991

[6] Primdahl, F.; The Fluxgate Mechanism, Part I: The Gating Curves of Parallel and Orthogonal Fluxgates. *IEEE Transactions on Magnetics*, Vol. MAG-6, Iss. 2, 1970, pp. 376-383

[7] Sasada, I.; Orthogonal fluxgate mechanism operated with dc bias excitation. *Journal of Applied Physics*, Vol. 91, Iss. 10, 2002, pp. 7789-7791, ISSN 0021-8979

[8] J.L.M.J. Van Bree, J.A. Poulis, F.N. Hooge; Barkhausen Noise in Fluxgate Magnetometers. *Applied Scientific Research*, Vol. 29, Iss. 1, 1974, pp. 59-68

[9] Butta M., Sasada I.: Method for offset suppression in orthogonal fluxgate with annealed wire core. *Sensor Letters*. 2014, no. 12, p. 1295-1298

[10] Sasada, I.; Symmetric Response obtained with an Orthogonal Fluxgate Operating in Fundamental Mode. IEEE Transactions on Magnetics, Vol. 38, N. 5, 2002

[11] Bartington Instruments Mag-03 Datasheet; http://www.bartington.com/Literaturepdf/Datasheets/Mag-03%20DS0013.pdf

[12] Stefan Mayer Instruments oficial FL1-100 Datasheet; http://www.stefan-mayer.com/images/datasheets/Data-sheet_FL1-100.pdf

[13] LEMI-022 Three component analog/digital magnetometer Datasheet; http://www.lemisensors.com/wp-content/uploads/2016/02/LEMI-022_Datasheet.pdf

[14] Billingsley Aerospace & Defence TFM100-G2 Datasheet; http://magnetometer.com/wp-content/uploads/TFM100-G2-Spec-Sheet-February-2008.pdf

[15] Nishio, Y., Tohyama, F., Onishi, N.; The sensor temperature characteristics of a fluxgate magnetometer by a wide-range temperature test for a Mercury exploration satellite. *Measurement Science and Technology*, Vol. 18, 2007, pp. 2721-2730

[16] Cerman, A., Merayo, J.M.G., Brauer, P., Primdahl, F.; Self-Compensating Excitatin of Fluxgate Sensors for Space Magnetometers. *IEEE Instrumentation and Measurement Technology Conference Proceedings*, 2008. DOI: 10.1109/IMTC.2008.4547387

[17] Primdahl, F., Risbo, T. Et al.; In-flight spacecraft magnetic field monitoring using scalar/vector gradiometry. *Measurement Science and Technology*, Vol. 17, 2006, pp. 1563-1569

List of figures

Bibliography/Sources

[1] Butta M., Sasada I.: Method for offset suppression in orthogonal fluxgate with annealed wire core. Sensor Letters. 2014, no. 12, p. 1295-1298.

[2] Sasada I, Usui T.: Orthogonal Fluxgate Magnetometer Utilizing Bias Switching for Stable Operation, Sensors, 2003. Proceedings of IEEE, Vol. 1, 468 - 471 , 22-24 Oct. 2003

[3] Datasheet of AD9850: http://www.analog.com/media/en/technical-documentation/data-sheets/AD9850.pdf

Appendix

A: Flipping circuit schematic

1. Power stage

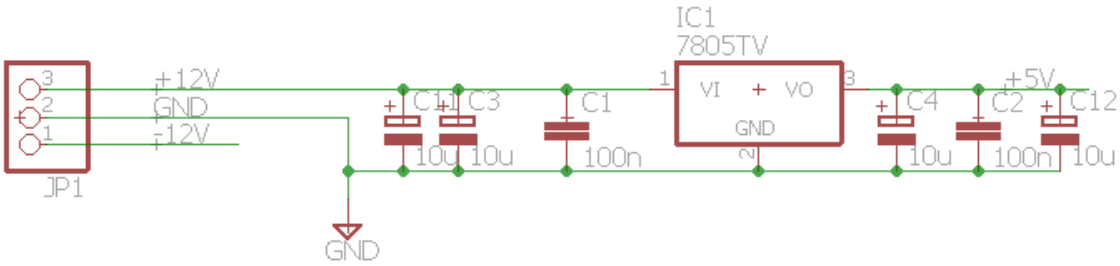

2: Connection of the frequency divider

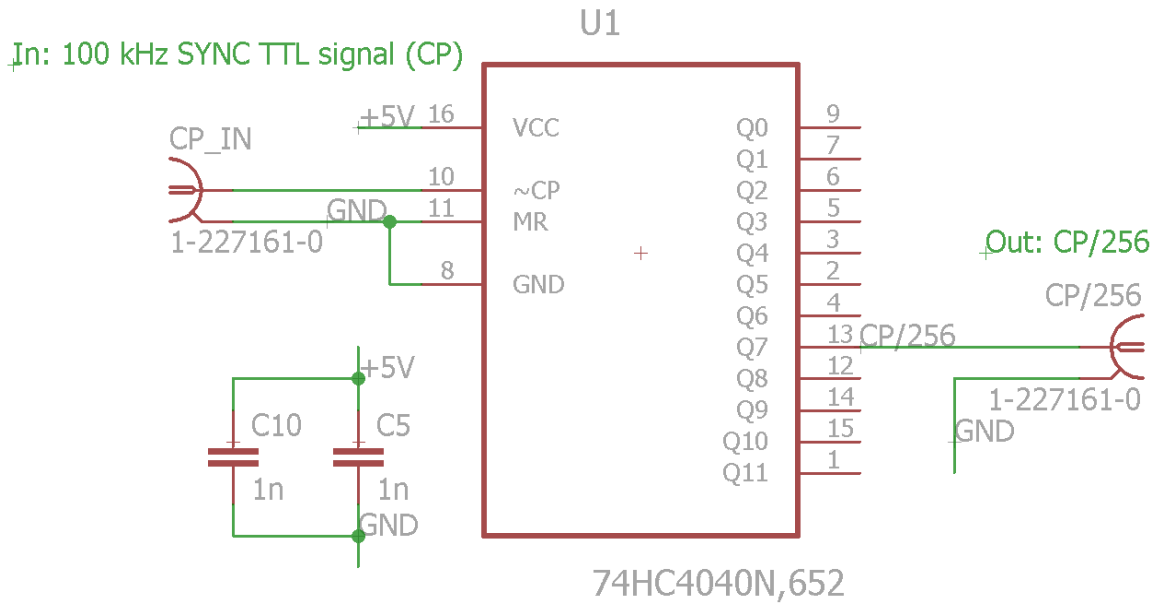

3: Connection of the NAND gate

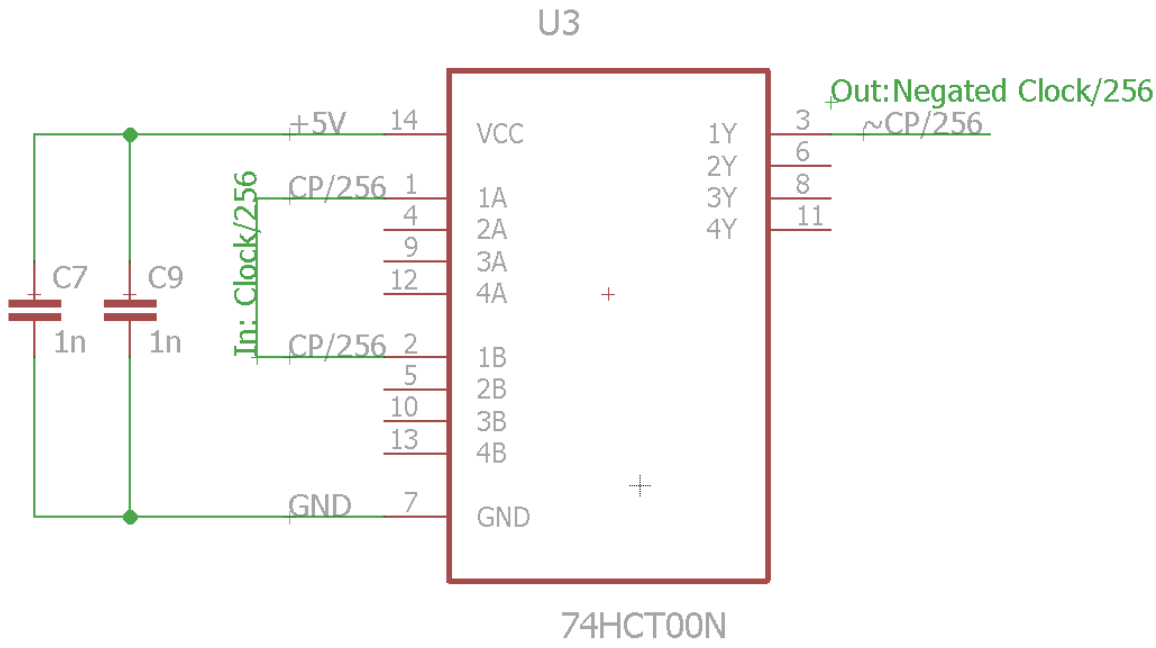

4. Connection of the solid state switches

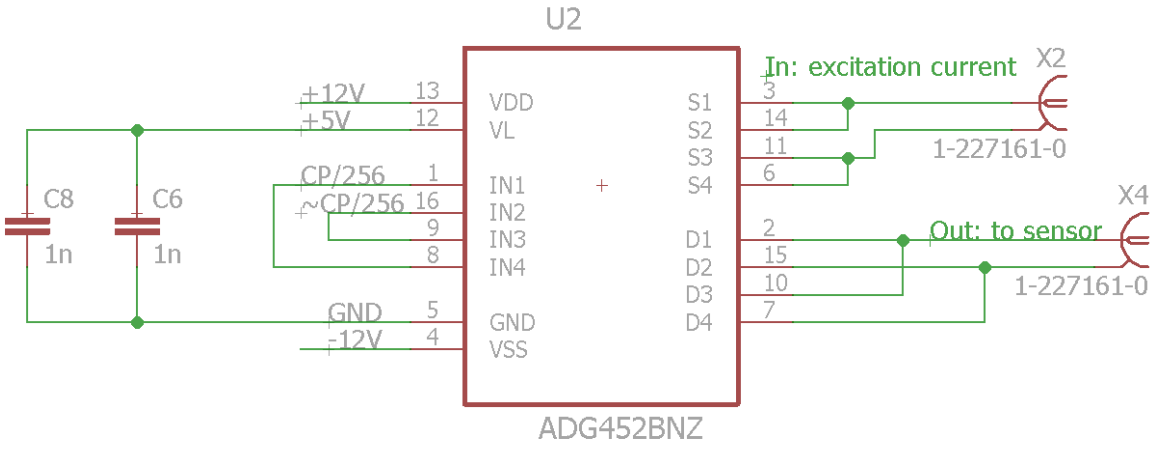

B: PCB of the flipping circuit

1. Top

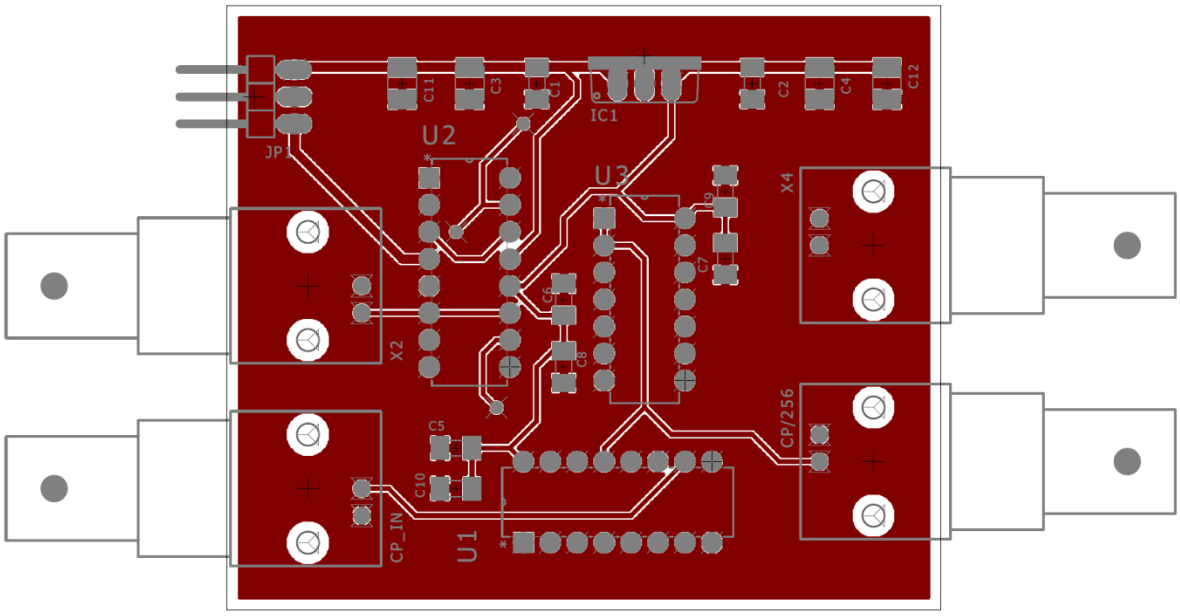

2. Bottom